



HAL
open science

An experimental and kinetic modeling study on the low-temperature oxidation of oxymethylene ether-2 (OME-2) by means of stabilized cool flames

Kevin de Ras, Thomas Panaget, Yann Fenard, Jeroen Aerssens, Laure Pillier, Joris Thybaut, Guillaume Vanhove, Kevin van Geem

► To cite this version:

Kevin de Ras, Thomas Panaget, Yann Fenard, Jeroen Aerssens, Laure Pillier, et al.. An experimental and kinetic modeling study on the low-temperature oxidation of oxymethylene ether-2 (OME-2) by means of stabilized cool flames. *Combustion and Flame*, 2023, 253, pp.112792. 10.1016/j.combustflame.2023.112792 . hal-04464815

HAL Id: hal-04464815

<https://hal.science/hal-04464815v1>

Submitted on 15 Nov 2024

HAL is a multi-disciplinary open access archive for the deposit and dissemination of scientific research documents, whether they are published or not. The documents may come from teaching and research institutions in France or abroad, or from public or private research centers.

L'archive ouverte pluridisciplinaire **HAL**, est destinée au dépôt et à la diffusion de documents scientifiques de niveau recherche, publiés ou non, émanant des établissements d'enseignement et de recherche français ou étrangers, des laboratoires publics ou privés.

An experimental and kinetic modeling study on the low-temperature oxidation of oxymethylene ether-2 (OME-2) by means of stabilized cool flames

Kevin De Ras^a, Thomas Panaget^{b,c,d}, Yann Fenard^b, Jeroen Aerssens^a, Laure Pillier^b,

Joris W. Thybaut^a, Guillaume Vanhove^b, Kevin M. Van Geem^{a,*}

^a Laboratory for Chemical Technology (LCT), Ghent University, Technologiepark-Zwijnaarde 125, B-9052 Ghent, Belgium

^b Université de Lille, CNRS, UMR 8522 – PC2A – Physicochimie des Processus de Combustion et de l'Atmosphère, F-59000 Lille, France

^c Université de Lille, Inserm, CHU Lille, Institut Pasteur Lille, U1167 – RID-AGE – Facteurs de risque et déterminants moléculaires des maladies liées au vieillissement, F-59000 Lille, France

^d Junia, Health and Environment, Laboratory of Sustainable Chemistry and Health, F-59000 Lille, France

* Corresponding author: Kevin.VanGeem@UGent.be, Technologiepark-Zwijnaarde 125, B-9052 Ghent, Belgium;

Keywords: Polyoxymethylene dimethyl ethers, Oxymethylene ether-2, Quantum chemistry, Kinetic modeling, Low-temperature oxidation, Stabilized cool flames.

Abstract:

Oxymethylene ethers have received much attention in recent years as a high-potential alternative for fossil-based fuels. These alternative fuels produced via carbon capture and utilization technologies driven by renewable energy can contribute to the solution of environmental issues in the short term. In this study, the low-temperature oxidation chemistry of oxymethylene ether-2 was investigated by combining experimental and kinetic modeling work. New experimental data were acquired from stabilized, ozone-seeded oxymethylene ether-2/dimethyl ether/oxygen premixed cool flames in a heated stagnation plate burner. Two fuel-lean equivalence ratios were investigated, i.e., $\phi = 0.3$ and $\phi = 0.5$. The observed and quantified reaction products were methoxymethyl formate, methyl formate, methanol, formaldehyde, CO and CO₂. A new detailed kinetic model based on first principles was constructed for the pyrolysis and oxidation of oxymethylene ether-2 with the in-house developed automatic kinetic model generation code Genesys. Compared to an earlier study by De Ras et al. (Combustion and Flame, 2022), additional species and reactions were added to describe the low-temperature oxidation chemistry with more detail, in addition to an update of several thermodynamic and kinetic parameters based on new quantum chemical calculations. The newly developed kinetic model is able to predict the experimental observations of the stabilized cool flames satisfactorily and can reproduce ignition delay times from the literature on average within the experimental uncertainty margin. Rate of production and sensitivity analyses were performed for different reaction conditions to unravel the important decomposition pathways during low-temperature oxidation. It is concluded that oxymethylene ether-2 is a highly reactive fuel, and this without fuel-specific chain branching reactions significantly contributing to the low-temperature oxidation chemistry.

1. Introduction

Significant ground-breaking research is currently ongoing to reach the so-called defossilization of the transportation sector by substituting fossil-based fuels with new (liquid) energy carriers. The latter are ideally produced in a sustainable manner, preferably using renewable resources such as biomass and green electricity, i.e., so-called biofuels and e-fuels [1, 2]. Polyoxymethylene dimethyl ethers (PODE), or more commonly referred to as oxymethylene ethers (OME), represent a class of molecules with alternating carbon and oxygen atoms in the backbone saturated with hydrogen atoms, corresponding to the structural formula $\text{CH}_3\text{O}(\text{CH}_2\text{O})_n\text{CH}_3$ (OME- n). These synthetic compounds can be produced starting from captured CO_2 via carbon capture and utilization (CCU) technology powered with renewable electricity, and would contribute to the development of the desired circular carbon economy in the short term [3-5]. Multiple engine studies already demonstrated that pure OME mixtures and OME-diesel blends enable cleaner combustion characteristics compared to conventional diesel fuels [6-13]. OMEs would result in, among other benefits, reduced particulate matter, due to the absence of carbon-carbon bonds in the fuel, and unburned hydrocarbon emissions while being compatible as a fuel additive for the current generation of diesel engines [10]. However, it is important to fully understand the low- and high-temperature combustion kinetics to promote the utilization of OMEs as sustainable e-fuels (or fuel additives) on a global scale. Especially, the low-temperature oxidation chemistry, which determines the auto-ignition characteristics of fuels, becomes more important in the development of more sustainable and cleaner combustion technologies, e.g., in the case of homogeneous charge compression ignition (HCCI) engines [14]. The development of detailed microkinetic models provides these fundamental insights into the decomposition chemistry and enables predictive simulations for

combustion applications. The present study builds further on an earlier publication by the same authors, which focused on the pyrolysis and oxidation of oxymethylene ether-2 (OME-2) [15], and is the first to investigate in more detail the low-temperature oxidation chemistry of OME-2. Despite OME-2 not being directly applicable as diesel fuel alternative due to its low boiling and flash point [10, 11], the obtained knowledge of this ‘model’ compound remains a prerequisite for development of new detailed microkinetic models for the more suitable OMEs, i.e., OME-3, OME-4 and OME-5 [16], in the future.

Meanwhile, several studies have been conducted to unravel the pyrolysis and oxidation chemistry of OME-2, both from an experimental and kinetic modeling point of view. Two sets of pyrolysis data acquired from tubular reactors were reported by De Ras et al. [15, 17] for different dilution ratios and pressures, covering a broad range of temperatures and residence times to explore both the primary and secondary chemistry. In addition, pyrolysis data for OME-2 from a jet-stirred reactor (JSR) were obtained by Zhong et al. [18]. More experimental data are available for the oxidation of OME-2. Ignition delay time (IDT) measurements were performed with OME-2/air mixtures in a shock tube (ST) by Cai et al. [19] for different equivalence ratios, and in a rapid compression machine (RCM) by De Ras et al. [15] and Drost et al. [20], for fuel-lean and stoichiometric mixtures, respectively. In addition, laminar burning velocity (LBV) measurements for OME-2/air mixtures covering a broad range of equivalence ratios were performed by Eckart et al. [21] with a heat flux burner, and by Ngugi et al. [22] with both a Bunsen cone flame burner and a shock tube. Recently, new oxidation experiments with a JSR were reported by Wang et al. [23] for different equivalence ratios, but the used experimental unit did not allow to quantify important products such as formaldehyde. Nevertheless, the number of available kinetic models in the literature focusing on the pyrolysis and oxidation chemistry of OME-2 is still limited. Multiple studies have focused on longer

OMEs [24] and were not explicitly validated for OME-2, despite it being an important aspect of the chemistry in these models, e.g., He et al. (OME-3) [25], Sun et al. (OME-3) [26] and Zhao et al. (OME-3) [27]. Cai et al. [19] has developed a kinetic model, which was validated against the IDT measurements from a ST for OME-2, OME-3 and OME-4. However, every previously mentioned kinetic model relies on extrapolations of thermodynamic and kinetic parameters from dimethyl ether (DME) and dimethoxymethane (DMM or OME-1) for longer OMEs, or on fitted parameters. The kinetic model developed by De Ras et al. [15] for pyrolysis and oxidation of OME-2 is the only available model based on first principles, which outperformed the other models from the literature. In the meantime, two additional studies were published by Van Geem and co-workers to refine this OME-2 model with new fundamental insights into the initial unimolecular decomposition pathways via carbene chemistry [17] and the radical decomposition of methoxymethyl formate and formic anhydride [28], i.e., important intermediates formed during pyrolysis and oxidation of OMEs.

In the present study, additional fundamental insights into the low-temperature oxidation chemistry of OME-2 were obtained by combined experimental and theoretical modeling work. Experiments were performed with stabilized, ozone-seeded OME-2/DME/O₂ premixed cool flames in a heated stagnation plate burner for lean and ultra-lean reaction conditions. Temperature and stable species mole fraction profiles along the burner axis were experimentally measured by coupling of thermocouples, gas chromatography and quadrupole mass spectrometry analyses. The experimental observations were compared with kinetic model simulation results. The in-house developed automatic kinetic model generation code Genesys [29] was used to construct a new elementary step kinetic model for the pyrolysis and oxidation of OME-2. This new kinetic model builds further on our earlier work [15] by including new reaction pathways for the low-temperature oxidation chemistry, in addition to an update of

several thermodynamic and kinetic parameters with quantum chemically calculated values. This is the first study to investigate the addition of hydroperoxy alkyl radicals of OME-2 to molecular oxygen and the associated decomposition pathways of hydroperoxyl alkyl peroxy radicals by means of quantum chemical calculations. The newly developed kinetic model was extensively validated with the acquired data from the cool flame burner and additional low-temperature oxidation data, i.e., IDT measurements, available from the literature. Rate of production and sensitivity analyses were carried out for different reaction conditions to unravel the important intermediate compounds and decomposition pathways during low-temperature oxidation.

2. Experimental methods

A heated stagnation plate burner configuration was used in the present study to acquire experimental data from stabilized, ozone-seeded OME-2/DME/O₂ premixed cool flames. The experimental unit was extensively described in previous studies [30, 31] and only the most important aspects are mentioned here.

The reactive mixtures were injected through a co-axial nozzle with an inner diameter of 10 mm, impinging a heated stagnation plate located 13 mm above the burner. The plate temperature was fixed at 600 K. A neat N₂ co-flow was injected via the co-axial nozzle to isolate the cool flame from external perturbations. The burner temperature was kept constant at 300 K using controlled-temperature water circulation. Liquid OME-2 (ASG Analytik-Service GmbH, purity > 98.5 mol%) was vaporized in the oxygen flow through a Controlled Evaporator Mixer (W-202-222-K, Bronkhorst). The liquid OME-2 flow rate was controlled by a Bronkhorst Coriolis mass flow controller. Gas flow rates of DME (Messer, purity 100 mol%), O₂ (Air Liquide, purity > 99.995 mol%) and N₂ (Air Liquide, purity > 99.995 mol%) were controlled

by Bronkhorst mass flow controllers. Ozone was generated using BMT 803 N and BMT 802 N ozone generators. The inlet mole fraction of ozone was measured using a Teledyne API 452 ozone analyzer. The relative uncertainty on the ozone measurements amounted to $\pm 0.02\%$ on the reported values. An ICCD Princeton PI-MAX 3, equipped with a band-pass filter (396 – 450 nm) was used to collect the excited formaldehyde (CH_2O^*) chemiluminescence signal of the cool flames. The obtained images were further processed via three-point Abel inversion [30] to extract axial CH_2O^* profiles and to precisely determine the cool flame positions. The latter is defined as the position above the burner at which the emission of CH_2O^* reaches a maximum. **Figure 1** shows a raw image of the CH_2O^* chemiluminescence signal from an ozone-seeded OME-2/DME/ O_2 premixed cool flame. A symmetric and flat cool flame is observed, positioned well below the heated stagnation plate.

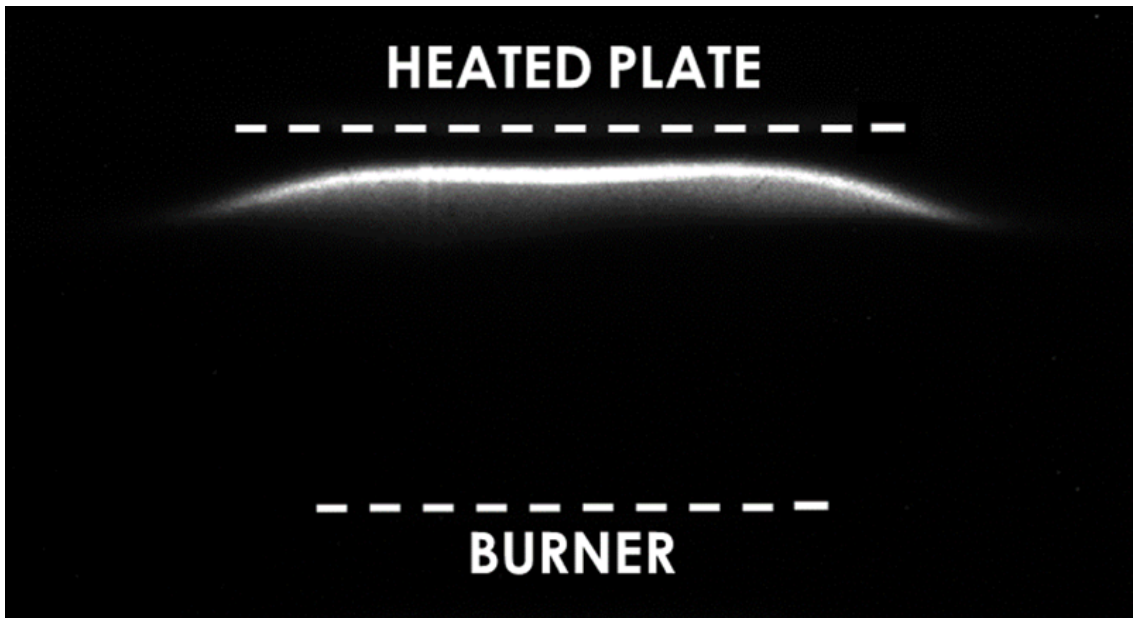


Fig. 1. Raw excited formaldehyde (CH_2O^*) chemiluminescence image of the stabilized, ozone-seeded OME-2/DME/ O_2 premixed cool flame for an equivalence ratio of $\phi = 0.5$, $x_{\text{O}_3} = 1.6$ mol% and a fixed geometric strain rate of 50 s^{-1} . The dashed lines represent the positions of the burner (bottom) and heated stagnation plate (top).

To investigate the decomposition pathways during OME-2 low-temperature oxidation, DME cool flames containing small quantities of OME-2 were studied with conditions close to those reported in earlier work by Panaget et al. [30]. OME-2 had to be seeded in DME, because of the low OME-2 vapor pressure and because the burner body was kept at room temperature. Two different fuel-lean equivalence ratios were selected, i.e., $\phi = 0.3$ and $\phi = 0.5$, for which the detailed experimental conditions are provided in **Table 1**. The geometric strain rate, defined as the ratio of the inlet velocity and the distance between the burner and heated plate, was kept fixed at 50 s^{-1} for both cool flames. As the equivalence ratio of the fuel mixture decreases, the required ozone mole fraction has to increase to stabilize the cool flame [30]. OME-1 was found to be the main impurity in the OME-2 fuel ($\approx 98.5 \text{ mol\% OME-2}$, 1.5 mol\% OME-1) and was therefore considered as part of the inlet feed for the kinetic model simulations [15].

Table 1. Experimental conditions for the stabilized, ozone-seeded OME-2/DME/O₂ premixed cool flames.

OME-2 / DME [mol% / mol%]	ϕ [-]	x_{O_3} [mol%]	x_{DME} [mol%]	$x_{\text{OME-2}}$ [mol%]	$x_{\text{OME-1}}$ [mol%]	x_{O_2} [mol%]	u_{inlet} [m s ⁻¹]
2.5 / 97.5	0.5	1.6	13.8	0.35	$5.32 \cdot 10^{-3}$	84.0	0.949
5 / 95	0.3	2.0	8.5	0.44	$6.68 \cdot 10^{-3}$	89.0	0.949

Temperature profiles were measured using a 250 μm diameter type-K thermocouple. Measurements were performed from the side of the burner with the tip of the thermocouple positioned along the axis of the burner. The absence of catalytic effects at the thermocouple surface was verified by measuring each temperature profile from the burner to the heated plate, and vice-versa [32], yielding nearly identical temperature profiles, as demonstrated in the Supplementary Material (Fig. 1S). The uncertainty margin for the temperature measurements is estimated to be $\pm 25 \text{ K}$. Radiative heat losses were neglected since the experimental maximal cool flame temperature typically does not exceed 900 K, which is below the frequently accepted

limit of 1000 K for this assumption [33]. Detailed major species mole fraction profiles were obtained by combining gas chromatography and quadrupole mass spectrometry techniques. Samples from the cool flames were extracted through a 220 μm external diameter capillary. The capillary was placed perpendicular to the burner axis. An Agilent 6890 gas chromatograph (GC), equipped with a ShinCarbon ST micropacked column, flame ionization and thermal conductivity detectors, was used to analyze the permanent gases. A Bruker SCION 456-GC, equipped with a PoraBond Q column, flame ionization and quadrupole detectors, was used for the identification and quantification of oxygenated products. The Bruker SCION 456-GC oven temperature program was set at 323 K (5 min hold) with a heating ramp of 10 K min^{-1} until 523 K (2 min hold) for a total runtime of 27 min. An Omnistar GSD 301 O₂ Pfeiffer Vacuum mass spectrometer, equipped with a quadrupole analyzer, was used to measure the ozone mole fraction profiles. Calibrations were performed with different techniques according to the availability of the different species, respectively by using commercial gas mixtures, in-house gas mixtures or the Equivalent Carbon Number (ECN) approach [34] when the species was unavailable. Reported experimental uncertainties are ± 5 mol% for calibrated species, ± 10 mol% for calibrated species with the ECN and ± 15 mol% for formaldehyde that was quantified from its peak on the mass spectrometer detector of the Bruker GC. The carbon balances were verified for both equivalence ratios, leading to a maximum deviation of ± 5 % downstream of the cool flames. The experimental product yields are provided in the Supplementary Material.

3. Computational methods

Quantum chemical calculations were performed at the CBS-QB3 level of theory [35] as implemented in Gaussian 16 [36]. Only the most important aspects of the computational methodology are discussed here, more details can be found in our earlier studies [15, 37].

The principles of ideal gas statistical thermodynamics were applied to calculate the thermodynamic parameters. To determine the lowest energy conformer, most likely geometries were optimized, followed by 1-dimensional rotational scans around single covalent bonds. In the case multiple diastereomers exist for a molecule, calculations were performed for all spatial possibilities, but only the geometry corresponding with the lowest energy was retained. The internal modes were approximated using the harmonic oscillators approach, except for internal modes corresponding to rotations around single covalent bonds. The latter were approximated by 1-dimensional hindered internal rotations (1D-HIR) if the electronic barrier did not exceed the threshold of 100 kJ mol⁻¹. The reduced moment of inertia calculated at the I^(2,3) level, as defined by East and Radom [38], combined with the Fourier series expression of the hindrance potential were used to construct the Schrödinger equation for a 1-dimensional internal rotation. The eigenvalues of this Schrödinger solution were used to construct the total partition function as function of the temperature from which thermodynamic parameters i.e., the standard enthalpy of formation (ΔH_f), the standard intrinsic entropy (S°) and heat capacities at constant pressure (C_p°), could be calculated. The enthalpies of formation at 298 K were obtained by using the atomization method with two additional corrections to adjust the calculated values for systematic errors. Firstly, spin-orbit corrections [39] as these are not yet included in the CBS-QB3 level of theory, and secondly, empirical bond additive corrections [40, 41] to correct for systematic deviations with experimental observations. If only relative energies were required, such as for calculating reaction rate coefficients and constructing potential energy surfaces, spin-orbit and bond additive corrections were not accounted for. Conventional transition state theory was applied to calculate the high-pressure limit reaction rate coefficients within the temperature range of 300 to 2000 K. The asymmetric Eckart potential was used to include the

effect of quantum chemical tunneling [42]. Modified Arrhenius parameters (A , n , E_a) were obtained by linear least-squares regression of reaction rate coefficients over the same temperature range.

Based on work by Paraskevas et al. [43], enthalpies of formation are assumed to be calculated within the chemical accuracy margin (4 kJ mol^{-1}) for non-radical compounds, and entropies are assumed to be well reproduced. Similar studies were conducted to evaluate the uncertainty on reaction rate coefficients calculated at the CBS-QB3 level of theory, incorporating Eckart tunneling and 1D-HIR corrections [44-46]. With this approach, it is assumed that the uncertainty of the kinetic parameters is within a factor of 2 to 4.

A list with all newly calculated thermodynamic and modified Arrhenius parameters at the CBS-QB3 level of theory, with accompanying the spatial coordinates of stable species and transition states, is provided in the Supplementary Material.

4. Kinetic model development

A kinetic model consisting of only elementary reaction steps was constructed for the pyrolysis and oxidation of OME-2. Both detailed low- and high-temperature oxidation chemistry is included in the reaction mechanism, but this study focused on the low-temperature oxidation chemistry of OME-2 under fuel-lean conditions.

The kinetic model was constructed using the in-house developed automatic model generation tool Genesys [29]. A number of initial species, a set of user-defined reaction families and associated constraints were specified as input to generate the reaction network. The used reaction families were adopted from our previous study on OME-2 [15]. However, additional reaction families were now implemented to describe the low-temperature oxidation chemistry in more detail. More in particular, the addition reactions of hydroperoxy alkyl radicals of

OME-2 to molecular oxygen were included, with associated the decomposition chemistry of the formed hydroperoxy alkyl peroxy radicals. The latter proceeds via intramolecular hydrogen abstractions, which can form keto hydroperoxides that decompose via homolytic scission of the oxygen-oxygen bond, or alkyl radicals that decompose by cyclic ether formation or β -scission reactions. To prevent unlimited extension of the reaction network, a rule-based termination criterion was applied. Constraints were specified based on our experience both on the level of reaction families and generated product species. For example, compounds with more than two double bonds are not included in the model, and cyclic ethers formed during low-temperature oxidation of OMEs can only decompose via low-activated unimolecular reactions (see further) and thus not via bimolecular hydrogen abstractions.

After constructing the reaction network, thermodynamic and kinetic parameters must be assigned to all species and reactions, respectively. Therefore, Genesys consists of user-defined databases, which contain thermodynamic and kinetic parameters generated from quantum chemical calculations. Such calculations were performed for species and reactions related to pathways believed to be important during the decomposition of OME-2. When there were no quantum chemical parameters available, thermodynamic parameters were calculated using Benson's group additivity method [47]. A new OME-specific group additivity scheme has been developed for thermodynamic parameters with the available OME data set. Given that quantum chemical kinetic parameters would be missing for a reaction, the kinetic group additivity method developed by Saeys et al. [48], rate rules or analogies from similar reactions were used to assign (modified) Arrhenius parameters. For OMEs, the hydrogen abstractions from different carbon atoms have been calculated for among others the hydrogen, methoxy, methyl, formyl, hydroperoxyl radical and molecular oxygen. From these results, rate rules have

been regressed, which were used in the case of similar reactive moieties. The kinetic group additivity scheme for oxygenated hydrocarbons determined by Paraskevas et al. [49] was used for the remaining hydrogen abstractions. For the low-temperature oxidation chemistry, almost all kinetic parameters were obtained from quantum chemical calculations. In the rare occasion that such calculations were not performed, kinetic parameters were assigned via reactivity-structure-based rate rules determined by Cai et al. [50] and Bugler et al. [51].

Finally, the generated kinetic model from Genesys for OME-2 was merged with a base mechanism, i.e., AramcoMech 1.3 [52]. This reaction mechanism contains 124 species and 766 reactions and describes the combustion chemistry of C₁-C₄ based hydrocarbons and oxygenated fuels, including DME. The kinetic model developed by Genesys does not include pressure-dependent kinetic parameters as a study by Aerssens et al. [53] has indicated that this pressure dependency is only important for smaller compounds in the low-temperature environment. The chemistry of smaller (oxygenated) hydrocarbons appears in the model via the base mechanism for which the pressure dependent kinetic parameters were fully adopted. In the case of conflicting thermodynamic or kinetic parameters during merging, the parameters from the AramcoMech mechanism were retained to maintain the integrity of this model, which has been validated over an extensive experimental database. The AramcoMech 1.3 mechanism was chosen over more recently extended versions [54-56] based on the experience of earlier studies by the authors and the limited size of this base mechanism, which excludes irrelevant chemistry. The newly developed kinetic model for pyrolysis and oxidation of OME-2 available in the Supplementary Material in CHEMKIN format consists of 376 species and 3988 reactions.

5. Results and discussion

5.1. Alkyl peroxy and hydroperoxy alkyl peroxy radicals

The oxidation of OME-2 is driven by a free radical mechanism. The oxidation chemistry is initiated via hydrogen abstractions from OME-2 by molecular oxygen. Two radicals can be formed, i.e., the primary radical (R_1^\bullet , $^\bullet\text{CH}_2\text{OCH}_2\text{OCH}_2\text{OCH}_3$) and the secondary radical (R_2^\bullet , $\text{CH}_3\text{OC}^\bullet\text{HOCH}_2\text{OCH}_3$). From a thermodynamic point of view, there is no favored formation of the secondary radical over the primary, as is the case for alkanes [15]. However, the calculated reaction rate coefficients indicate that formation of the secondary radical is favored. In the case of low-temperature oxidation, the formed OME-2 radicals can add to molecular oxygen to form alkyl peroxy radicals (ROO^\bullet), which can decompose further via low-temperature oxidation reaction pathways similar to alkanes. This includes among others intramolecular hydrogen abstractions, cyclic ether formations and β -scissions [57]. The addition reaction of radicals to molecular oxygen does not occur at higher temperatures as it is thermodynamically no longer preferred.

Thermodynamic parameters for the alkyl peroxy radicals, the alkyl hydroperoxy radicals ($^\bullet\text{QOOH}$) and the alkyl hydroperoxy species (ROOH) of OME-2 are provided in **Table 2** as obtained from quantum chemical calculations. Although the enthalpies of formation at 298 K of R_1^\bullet and R_2^\bullet only differ by 1 kJ mol^{-1} , the difference in the enthalpies of formation of $R_1\text{OO}^\bullet$ and $R_2\text{OO}^\bullet$ amounts to 12.5 kJ mol^{-1} . The formed carbon-oxygen bond in the case of the secondary carbon radical is thus significantly stronger. When looking at the associated hydroperoxy species, i.e., $R_1\text{OOH}$ and $R_2\text{OOH}$, it is observed that the latter is only 7.8 kJ mol^{-1} more stable. In addition, the peroxy functional group does not disturb the favorable helix-like

structure of consecutive oxymethylene units as can be seen from **Fig. 2**, which depicts the lowest energy conformers. In the case of a hydroperoxy functional group, intramolecular hydrogen bonds are favored, which reduce the electronic energy of the molecule by stabilization, but these also reduce the entropy significantly. As depicted in **Fig. 2**, the lowest energy conformer of R_1OOH still preserves this helix-like structure with favorable gauche interactions, but in the case of R_2OOH this structure is distorted by a part of the backbone, which has a planar configuration. For both hydroperoxides, the formed hydrogen bonds result in seven-membered ring structures. The decomposition of the alkyl hydroperoxy radicals has been investigated in our previous study by means of potential energy surfaces [15] and is therefore not repeated here. $R_1OO\bullet$ can isomerize via intramolecular hydrogen abstractions to form $\bullet Q_{1,2}OOH$, $\bullet Q_{1,3}OOH$ and $\bullet Q_{1,4}OOH$. The enthalpies of formation of the latter radicals are very similar and only differ by 6.6 kJ mol^{-1} at maximum. However, differences in the entropy values are more pronounced. These can be partly explained since $\bullet Q_{1,2}OOH$ and $\bullet Q_{1,3}OOH$ form nine-membered ring structures due to intramolecular hydrogen bonds and $\bullet Q_{1,4}OOH$ forms a smaller seven-membered ring structure. Similarly, $R_2OO\bullet$ can isomerize to form $\bullet Q_{2,1}OOH$, $\bullet Q_{2,3}OOH$ and $\bullet Q_{2,4}OOH$. The difference in the enthalpies of formation between these isomers remains in the range of 3.7 kJ mol^{-1} . Hydrogen bonds are observed in the lowest energy conformers forming seven-membered ring structures for $\bullet Q_{2,1}OOH$ and $\bullet Q_{2,3}OOH$. The optimal geometry of $\bullet Q_{2,4}OOH$ deviates as the hydroperoxyl functionality interacts with the carbon radical instead of an oxygen atom to form an eight-membered ring structure. Lowest energy conformers of the alkyl hydroperoxy radicals are provided in the Supplementary Material (Fig. 2S). Note that although the enthalpies of formation are expected to be reproduced within the

uncertainty margin of 4 kJ mol^{-1} , the error on enthalpy differences is expected to be less due to the cancellation of systematic errors of the quantum chemical calculations.

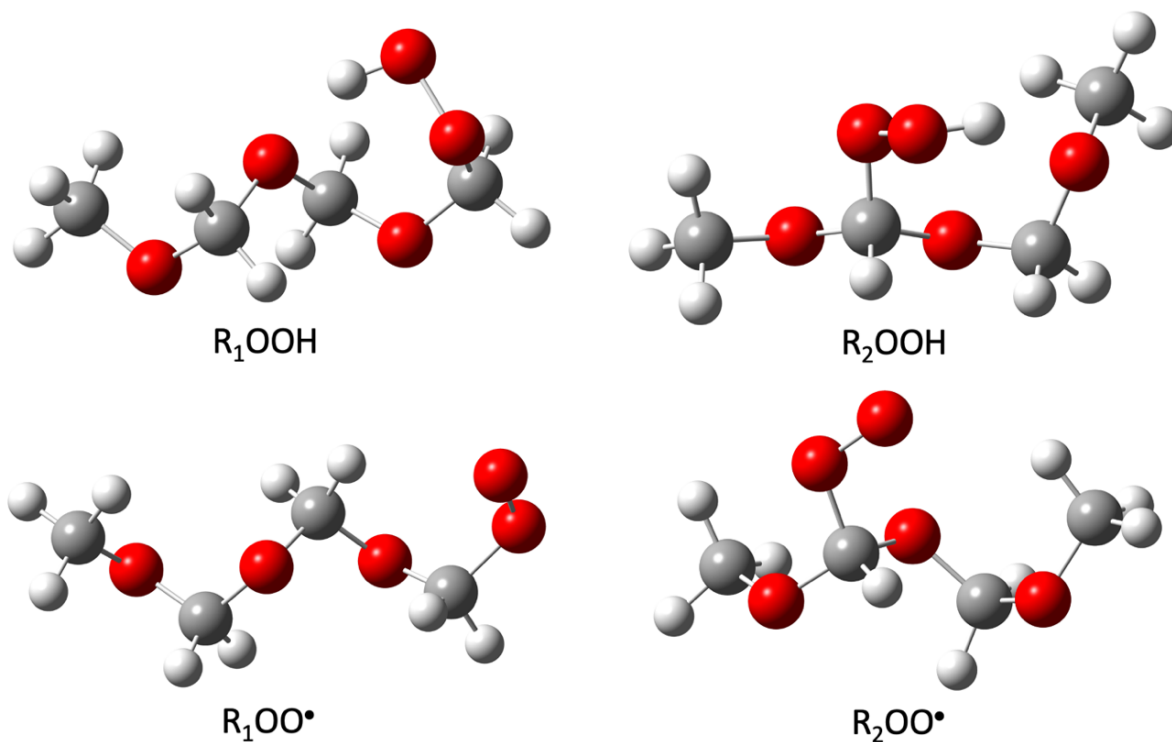
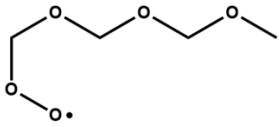
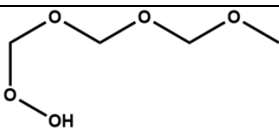
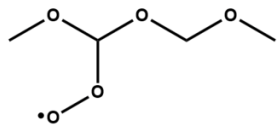
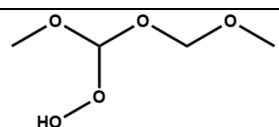
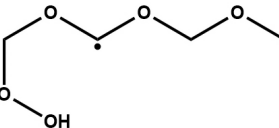
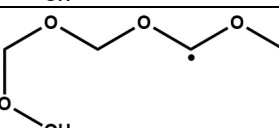
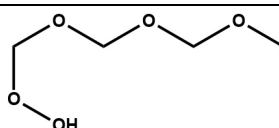
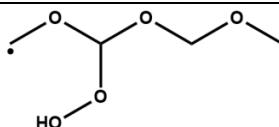
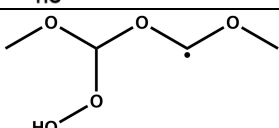
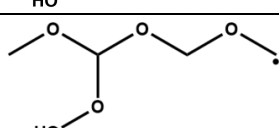


Fig. 2. Lowest energy conformers at the CBS-QB3 level of theory of the alkyl hydroperoxy species (top, R_1OOH and R_2OOH) and the alkyl peroxy radicals (bottom, R_1OO^\bullet and R_2OO^\bullet) of OME-2.

Table 2. Molecular structures and thermodynamic properties, i.e., standard enthalpies of formation (ΔH_f°) and entropies (S°) at 298 K and heat capacities (C_p°) at 300, 500 and 1000 K, of the alkyl peroxy radicals (ROO^\bullet), alkyl hydroperoxy radicals ($^\bullet\text{QOOH}$) and alkyl hydroperoxy species (ROOH) of OME-2 obtained at the CBS-QB3 level of theory.

Species	Structure	ΔH_f° [kJ mol ⁻¹]	S° [J mol ⁻¹ K ⁻¹]	C_p° [J mol ⁻¹ K ⁻¹]		
				300 K	500 K	1000 K
$\text{R}_1\text{OO}^\bullet$		-468.7	459.2	176.5	247.9	324.5
R_1OOH		-634.4	427.8	168.0	252.6	363.5
$\text{R}_2\text{OO}^\bullet$		-481.2	454.6	167.1	238.4	332.7
R_2OOH		-642.2	428.0	169.6	246.7	353.0
$^\bullet\text{Q}_{1,2}\text{OOH}$		-435.9	410.8	159.3	244.3	365.8
$^\bullet\text{Q}_{1,3}\text{OOH}$		-442.5	420.0	162.6	241.3	360.6
$^\bullet\text{Q}_{1,4}\text{OOH}$		-439.0	428.8	174.0	253.9	351.5
$^\bullet\text{Q}_{2,1}\text{OOH}$		-444.1	426.8	177.3	249.9	343.4
$^\bullet\text{Q}_{2,3}\text{OOH}$		-445.9	443.2	171.7	246.3	345.8
$^\bullet\text{Q}_{2,4}\text{OOH}$		-447.8	426.7	182.8	256.1	351.1

Each alkyl hydroperoxy radical of OME-2 can react further via an addition to molecular oxygen to form hydroperoxy alkyl peroxy radicals ($\bullet\text{OOQOOH}$), typically under fuel-lean reaction conditions. In the case of alkanes, these are the reactions leading to an acceleration of the reactivity at low temperatures due to additional radicals being formed via chain branching reactions. Thermodynamic properties of the hydroperoxy alkyl peroxy radicals are provided in **Table 3**. This is the first study to report parameters for these compounds based on quantum chemical calculations. Due to the peroxy and hydroperoxy functionalities, a lot of intramolecular interactions become possible, which required a multitude of calculations to find and verify lowest energy conformers. The geometry of each isomer in its lowest energy conformer is depicted in **Fig. 3**. Both the thermodynamic properties and geometries differ significantly among different isomers. For four of the six isomers, a hydrogen bond is formed between the hydroperoxy and peroxy functional group. In the case of $\bullet\text{OOQ}_{1,2}\text{OOH}$, $\bullet\text{OOQ}_{2,1}\text{OOH}$ and $\bullet\text{OOQ}_{2,3}\text{OOH}$, this creates an eight-membered ring structure. In the case of $\bullet\text{OOQ}_{2,4}\text{OOH}$, a ten-membered ring structure is formed. A larger cyclic structure reduces the freedom of movement and thus the disorder in the molecule, which explains the lower entropy of $\bullet\text{OOQ}_{2,4}\text{OOH}$. $\bullet\text{OOQ}_{2,3}\text{OOH}$ is the most stable isomer with an enthalpy of formation at 298 K of $-613.6 \text{ kJ mol}^{-1}$, more than 15 kJ mol^{-1} difference compared to the second most stable isomer. The methoxymethoxy structure that does not interact with the peroxy, nor hydroperoxy functionality in $\bullet\text{OOQ}_{1,2}\text{OOH}$ and $\bullet\text{OOQ}_{2,1}\text{OOH}$ preserves the favored gauche interactions. Only in the cases of $\bullet\text{OOQ}_{1,3}\text{OOH}$ and $\bullet\text{OOQ}_{1,4}\text{OOH}$, the hydrogen atom of the hydroperoxy functionality interacts with an oxygen atom from the OME-2 chain instead of the peroxy group, which results in seven-membered ring structures. For $\bullet\text{OOQ}_{1,3}\text{OOH}$, the peroxy functionality is undisturbed and does not seem to be influenced by intramolecular interactions. This isomer has

therewith the highest entropy value and stands out significantly compared to the other isomers. For $\bullet\text{OOQ}_{1,4}\text{OOH}$, the chain is extremely coiled to form a hydrogen bond between the hydroperoxy group and an oxygen atom in the chain, but also to have some intramolecular interaction between the hydroperoxyl and peroxy group. Despite these interactions, this isomer is the least favorable and has the highest enthalpy of formation. Coiling also results in a significant reduction of the entropy. All these intramolecular interactions are hard for a group additivity scheme to capture and make it difficult to provide results within the chemical accuracy margin, even when introducing non- next-nearest neighbor interactions [58]. For example, $\bullet\text{OOQ}_{1,2}\text{OOH}$ and $\bullet\text{OOQ}_{1,3}\text{OOH}$ consist of the same molecular groups according to Benson's group additivity theory but the enthalpy of formation and entropy differ by more than 10 kJ mol^{-1} and $20 \text{ J mol}^{-1} \text{ K}^{-1}$, respectively. Note that for $\bullet\text{OOQ}_{2,3}\text{OOH}$ different diastereomers exist as the molecule has two chiral centers. The difference in electronic energy between the two diastereomers amounts to 8.4 kJ mol^{-1} . Only the most stable geometry was considered for the kinetic model. For the other isomers, only enantiomers exist which have identical thermodynamic properties.

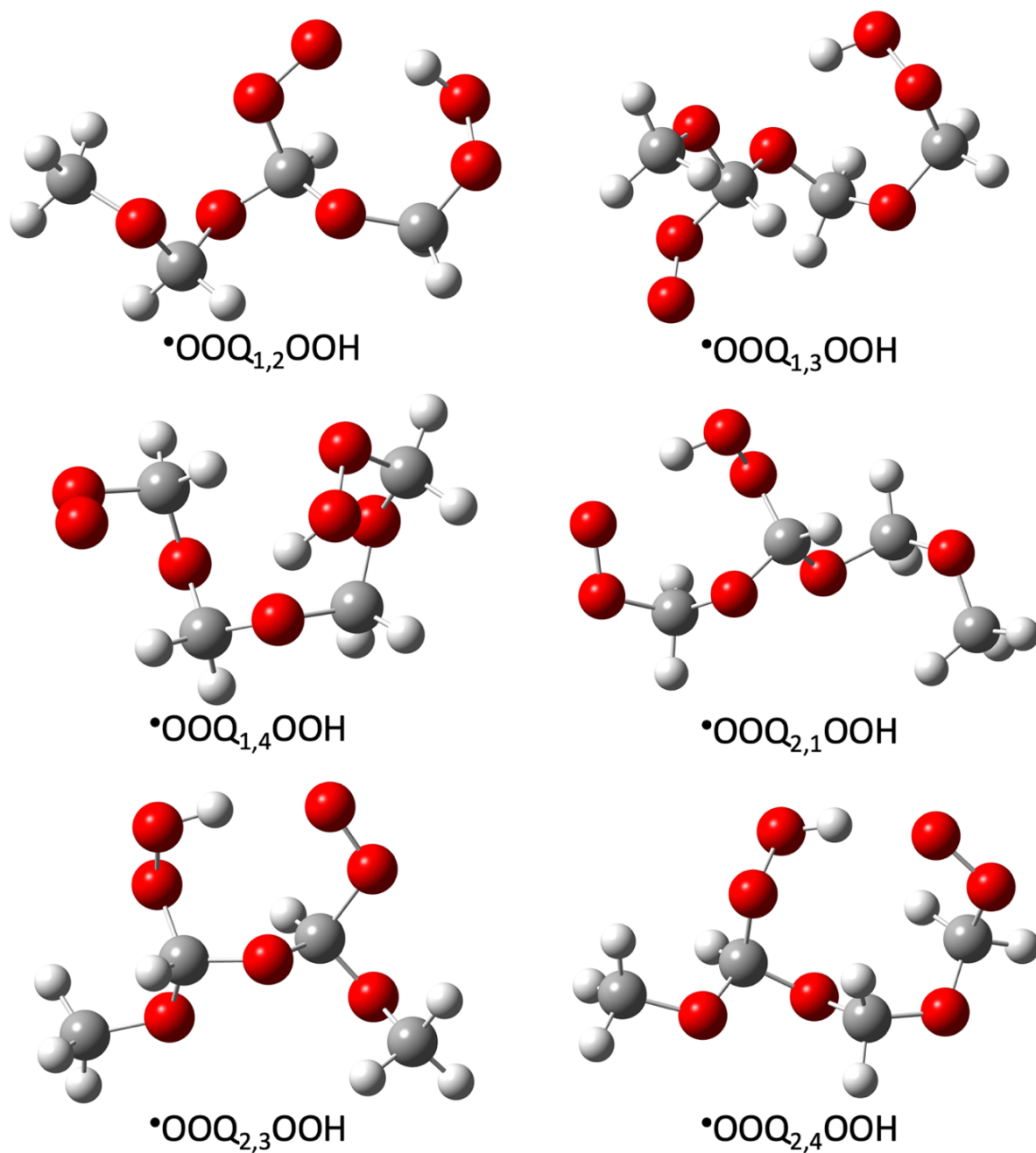


Fig. 3. Lowest energy conformers at the CBS-QB3 level of theory of the hydroperoxy alkyl peroxy radicals of OME-2 ($\bullet\text{OOQ}_{1,2}\text{OOH}$, $\bullet\text{OOQ}_{1,3}\text{OOH}$, $\bullet\text{OOQ}_{1,4}\text{OOH}$, $\bullet\text{OOQ}_{2,1}\text{OOH}$, $\bullet\text{OOQ}_{2,3}\text{OOH}$ and $\bullet\text{OOQ}_{2,4}\text{OOH}$).

Table 3. Molecular structures and thermodynamic properties, i.e., standard enthalpies of formation (ΔH_f°) and entropies (S°) at 298 K and heat capacities (C_p°) at 300, 500 and 1000 K, of the hydroperoxy alkyl peroxy radicals ($\bullet\text{OOQOOH}$) of OME-2 obtained at the CBS-QB3 level of theory.

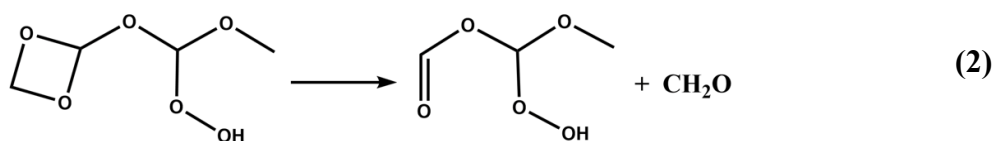
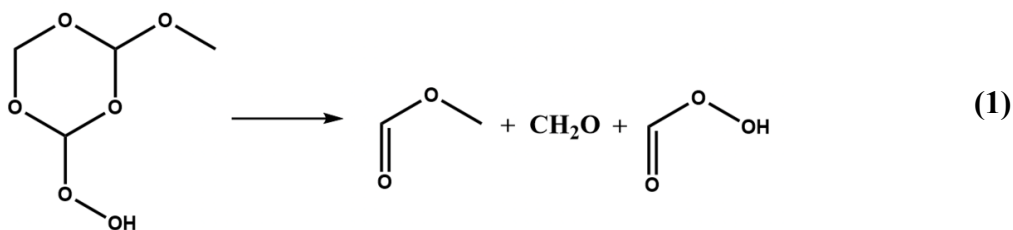
Species	Structure	ΔH_f° [kJ mol ⁻¹]	S° [J mol ⁻¹ K ⁻¹]	C_p° [J mol ⁻¹ K ⁻¹]		
				300 K	500 K	1000 K
$\bullet\text{OOQ}_{1,2}\text{OOH}$		-587.1	479.0	200.4	288.1	394.6
$\bullet\text{OOQ}_{1,3}\text{OOH}$		-598.1	499.1	196.6	283.6	389.8
$\bullet\text{OOQ}_{1,4}\text{OOH}$		-586.5	468.2	191.9	278.5	388.2
$\bullet\text{OOQ}_{2,1}\text{OOH}$		-598.2	471.7	198.2	291.9	406.9
$\bullet\text{OOQ}_{2,3}\text{OOH}$		-613.6	485.2	202.5	280.3	389.9
$\bullet\text{OOQ}_{2,4}\text{OOH}$		-596.4	465.3	192.0	282.3	426.4

5.2. Potential energy surfaces for low-temperature oxidation

Six different isomers can be formed by the addition of alkyl hydroperoxyl radicals of OME-2 to molecular oxygen, their decomposition chemistry is discussed in detail in this section and the Supplementary Material. The investigated decomposition pathways, i.e., intramolecular hydrogen abstractions, β -scissions and cyclic ether formation reactions, of each isomer were investigated by construction of the potential energy surfaces.

The potential energy surface for $\bullet\text{OOQ}_{2,3}\text{OOH}$ is depicted in Fig. 4. The values represent enthalpies of formation at 0 K, i.e., electronic energies, at the CBS-QB3 level of theory relative to $\bullet\text{OOQ}_{2,3}\text{OOH}$. The barrierless addition of molecular oxygen to $\bullet\text{Q}_{2,3}\text{OOH}$ to form $\bullet\text{OOQ}_{2,3}\text{OOH}$ is associated with an electronic reaction enthalpy of $167.0 \text{ kJ mol}^{-1}$. The $\bullet\text{OOQ}_{2,3}\text{OOH}$ radical can react further via two intramolecular hydrogen abstractions. The first is a hydrogen shift from a primary carbon atom to the peroxy group, which can proceed via a six-membered and an eight-membered transition state with an electronic barrier of 84.8 and 91.2 kJ mol^{-1} , respectively. The formed hydroperoxy alkyl hydroperoxy radical is 45.8 kJ mol^{-1} higher in electronic energy. The energetically most favorable decomposition pathway for this radical is via the cyclic ether formation of a six-membered ring structure, i.e., 2-methoxy-4-hydroperoxide-1,3,5-trioxane, and the hydroxyl radical with an electronic barrier of 73.5 kJ mol^{-1} . The alkyl radical can also decompose via β -scission with simultaneously a molecular rearrangement of the $\bullet\text{COOH}$ functionality with the formation of formaldehyde, 2-hydroperoxymethoxymethyl formate and the hydroxyl radical. This corresponds with an electronic reaction barrier of 79.4 kJ mol^{-1} and forms a keto hydroperoxyl species. A third reaction pathway is again cyclic ether formation with the formation of methoxy(hydroperoxymethoxy) substituted 1,3-dioxetane, and the hydroxyl radical. The latter reaction corresponds with an electronic reaction barrier of 85.7 kJ mol^{-1} but forms a tight four-membered cyclic ether, which creates a lot of ring strain and reduces the electronic reaction enthalpy. The formed cyclic ethers can decompose via unimolecular decomposition reactions in which consecutive carbon-oxygen bonds are broken and transformed into double bonds. For example, 2-methoxy-4-hydroperoxide-1,3,5-trioxane can decompose into formaldehyde,

methyl formate and methaneperoxoic acid as described by **Reaction (1)**. The corresponding electronic reaction barrier and enthalpy amount to 137.4 and -122.7 kJ mol⁻¹, respectively.



Note that in the case of unimolecular decomposition of the four-membered cyclic ether, as described by **Reaction (2)**, identical reaction products are formed as the β -scission reaction. Keto hydroperoxyl compounds can thus also be formed via the decomposition of the cyclic ethers. This leads to chain branching reactions as the keto hydroperoxide can split into two radicals by homolytic scission of the unstable oxygen-oxygen bond and there is an additional hydroxyl radical formed during the cyclic ether formation. Such reactions, in which one radical decomposes and leads to three radicals during low-temperature oxidation are well-known to lead to a significant increase of the reactivity in the case of alkanes. The formation and unimolecular decomposition of cyclic ethers as such enhances the reactivity by chain branching and due to the exothermicity of releasing ring strain by formation of multiple energetically favorable carbonyl functionalities, as demonstrated in our previous study [15]. $\bullet\text{OOQ}_{2,3}\text{OOH}$ can undergo a hydrogen shift from the two tertiary carbon atoms to the peroxy group, which can proceed via a tight four-membered or six-membered transition state, with associated electronic reaction barriers of 171.4 and 88.8 kJ mol⁻¹, respectively. A keto hydroperoxyl species is formed, which can again lead to chain branching reactions. For $\bullet\text{OOQ}_{2,3}\text{OOH}$, it is seen that the hydrogen shift via the six-membered transition state is the most favorable

decomposition pathway with a significantly lower electronic barrier ($>30 \text{ kJ mol}^{-1}$) compared to the other pathways, which is also associated with the largest electronic reaction enthalpy, i.e., $-193.5 \text{ kJ mol}^{-1}$, of the considered reactions. In the case of intramolecular hydrogen abstraction by the peroxy group from the hydroperoxy group of $\bullet\text{OOQ}_{2,3}\text{OOH}$, the same molecule is formed due to the molecular symmetry, which is therefore not depicted.

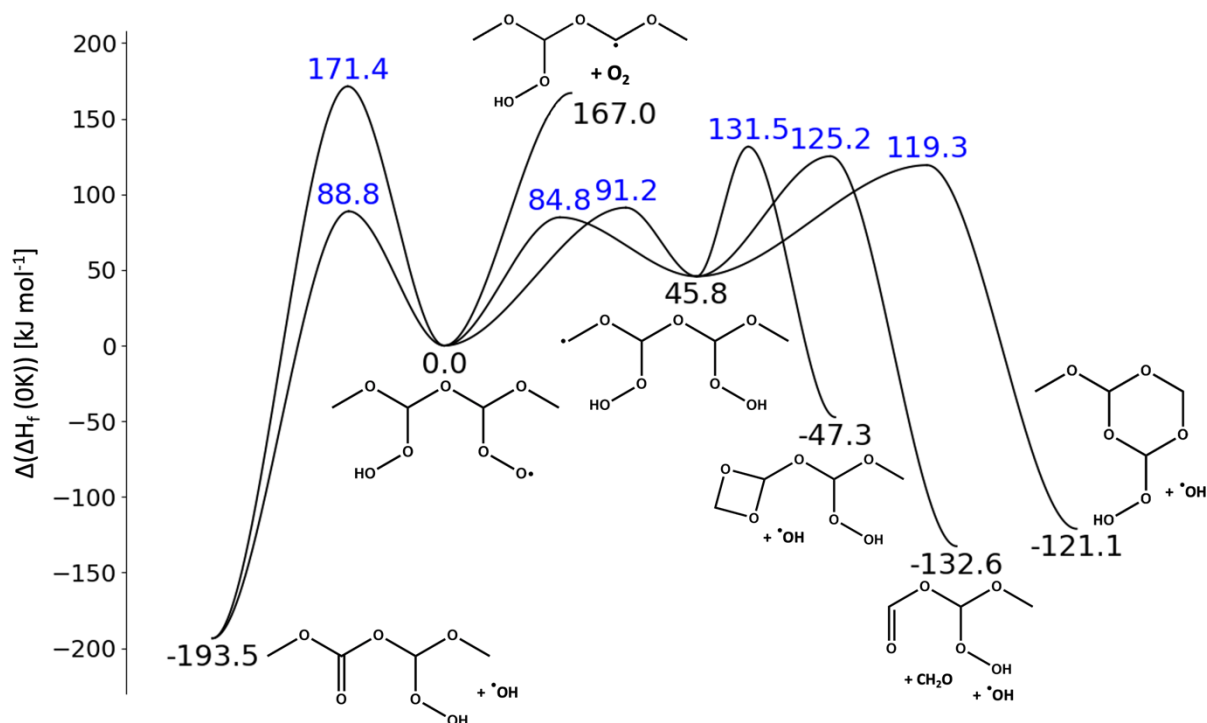


Fig. 4. Selected part of the potential energy surface for the addition of molecular oxygen to $\bullet\text{Q}_{2,3}\text{OOH}$. The values are enthalpies of formation calculated at the CBS-QB3 level of theory at 0 K relative to $\bullet\text{OOQ}_{2,3}\text{OOH}$. Blue and black numbers indicate values for the transition states and stable species, respectively.

The potential energy surface for $\bullet\text{OOQ}_{1,4}\text{OOH}$ is shown in **Fig. 5**. The $\bullet\text{OOQ}_{1,4}\text{OOH}$ radical is formed after addition of molecular oxygen to $\bullet\text{Q}_{1,4}\text{OOH}$ associated with an electronic reaction enthalpy of $146.2 \text{ kJ mol}^{-1}$. Like the case of $\bullet\text{OOQ}_{2,3}\text{OOH}$, the decomposition of the formed hydroperoxy alkyl peroxy radical is initiated with intramolecular hydrogen abstractions for which two possibilities exist. The first one is a hydrogen shift from a secondary carbon atom

to the peroxy group via a six-membered or eight-membered cyclic transition state with electronic reaction barriers of 69.4 and 79.6 kJ mol⁻¹, respectively. The formed dihydroperoxy alkyl radical with four possible decomposition pathways has an electronic energy difference of only 29.1 kJ mol⁻¹ compared to $\bullet\text{OOQ}_{1,4}\text{OOH}$. Two β -scissions are possible. The first forms hydroperoxymethoxymethyl formate, formaldehyde and the hydroxyl radical, via a transition state with an electronic barrier of 63.2 kJ mol⁻¹. For the other β -scission, the electronic barrier amounts to 58.8 kJ mol⁻¹ to form hydroperoxymethyl formate and the hydroperoxymethoxymethyl radical, but these reaction products are higher in energy and thus less stable compared to $\bullet\text{OOQ}_{1,4}\text{OOH}$. However, these products can rapidly lead to the formation of more stable compounds, i.e., mostly formaldehyde, by β -scissions and homolytic scissions. In addition, two cyclic ether formation pathways are possible via a four-membered and six-membered transition states with barriers of 82.8 and 56.4 kJ mol⁻¹, respectively. The formation of the 1,3,5-trioxane derivative is again favored compared to the tight four-membered cyclic ether structure. Decomposition of the four-membered cyclic ether leads to identical products as the most favorable β -scission. Another hydrogen shift in $\bullet\text{OOQ}_{1,4}\text{OOH}$ from an end-standing secondary carbon atom to a peroxy group, directly associated with a molecular rearrangement, proceeds via a four-membered or an eight-membered transition state with electronic barriers of 159.5 and 78.9 kJ mol⁻¹, respectively. This eight-membered transition state is electronically the most favorable reaction of all decomposition pathways. However, it is highlighted that compared to the decomposition of $\bullet\text{OOQ}_{2,3}\text{OOH}$ (**Fig. 4**), the latter hydrogen shift is only slightly favored as another decomposition pathway is already possible with a transition state only 9 kJ mol⁻¹ higher in electronic energy. An intramolecular hydrogen

abstraction between the peroxy and hydroperoxy functionality of $\bullet\text{OOQ}_{1,4}\text{OOH}$ leads to an identical structure as was the case for $\bullet\text{OOQ}_{2,3}\text{OOH}$.

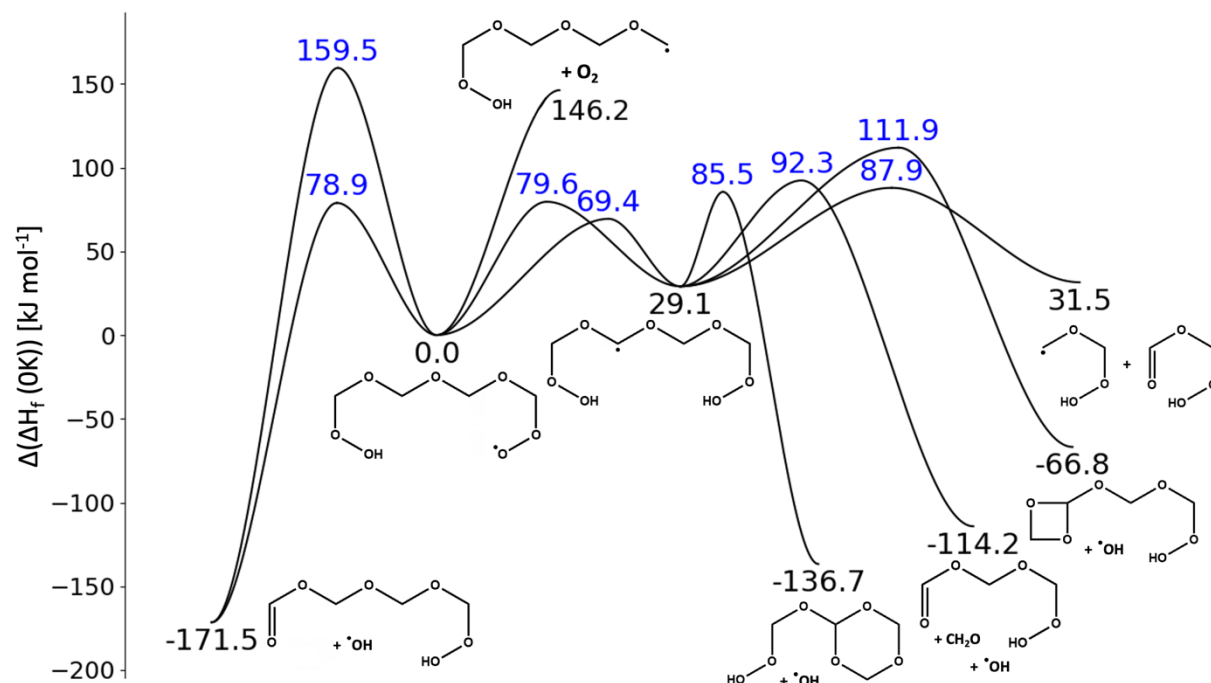


Fig. 5. Selected part of the potential energy surface for the addition of molecular oxygen to $\bullet\text{Q}_{1,4}\text{OOH}$. The values are enthalpies of formation calculated at the CBS-QB3 level of theory at 0 K relative to $\bullet\text{OOQ}_{1,4}\text{OOH}$. Blue and black numbers indicate values for the transition states and stable species, respectively.

The potential energy surfaces for the other hydroperoxy alkyl peroxy radicals of OME-2 and associated discussion of the results can be found in the Supplementary Material (Fig. S3 up to Fig. S6). Some general conclusions can be made based on the constructed potential energy surfaces. Due to the characteristic structure of OMEs, the cyclic ethers that can be formed always consist of an even number of atoms with an equal amount of oxygen and carbon atoms in the cyclic structure. The four-membered cyclic ethers are typically more difficult to form by a higher activated transition state compared to six- and eight-membered cyclic ethers due to the larger ring strain. Moreover, it was found that for the discussed four-membered cyclic ethers in

this study, the trans configuration is always the most stable one due to less steric hindrance. Associated, the transition states to form these cyclic ethers also favor the trans configuration. The decomposition of hydroperoxy alkyl peroxy radicals results in a multitude of products that always form keto hydroperoxyl species, either directly via intramolecular hydrogen abstractions and β -scissions, or indirectly via decomposition of the cyclic ethers. The products formed during low-temperature oxidation of OME-2 are therefore very similar independent of the followed decomposition pathway.

5.3. Stabilized, ozone-seeded OME-2/DME/O₂ premixed cool flames

The stabilized cool flames were simulated using the impinging-jet reactor class from Cantera, with multicomponent transport data. The energy equation was solved during the simulations and the experimental temperature profiles were as such not used as input. A submechanism describing the ozone decomposition was added to the kinetic model for OME-2. Among the different ozone submechanisms published in the literature, the recently published model from Jian et al. [59] was chosen. For the transport properties of the molecules, the data available from the AramcoMech 1.3 base mechanism were used. When data were not available from this mechanism, it was calculated using empirical correlations based on the molar mass of the molecule as reported by Wang and Frenklach [60]. For the smallest species, all transport properties could be found in the base mechanism. An input file containing the transport properties for the newly developed OME-2 model is provided in the Supplementary Material in CHEMKIN format.

5.3.1. Experimental results and kinetic model simulations

An important product formed by β -scissions in the thereby investigated ozone-seeded OME-2/DME/O₂ premixed cool flames is formaldehyde. Although this species would fully decompose in so-called hot flames, it is formed as a stable oxidation product in the temperature range of the cool flame. Formaldehyde can be formed in an excited electronic state (CH₂O*) and evolve rapidly to the electronic ground state in the flame front accompanied by chemiluminescence, causing the cool flames to faint light emissions. This enables the precise determination of the position of the cool flame without perturbation induced by the measurement microprobe.

In **Fig. 6**, the measured and model predicted temperature profiles are compared as a function of the height above burner (HAB) for the cool flames with equivalence ratios of $\phi = 0.3$ (left, $x_{O_3} = 2.0$ mol%) and $\phi = 0.5$ (right, $x_{O_3} = 1.6$ mol%). The cool flame front position is slightly lower in the case of an equivalence ratio of $\phi = 0.3$ in comparison to the case of $\phi = 0.5$, which is well captured by the modeling results. However, the position of the cool flame front is overpredicted by the model, as visible from the steep increase in the simulated temperature profile. The perturbation of the cool flame by the thermocouple explains part of this discrepancy, as confirmed when comparing the maximal chemiluminescence signal with the maximal experimental temperature gradient. Therefore, a steeper increase of the temperature is predicted by the model compared to the experimental measurement. Nonetheless, a good agreement is observed for the maximal temperature reached for the experimental and model simulated results, which stays below 900 K. Comparable maximal temperatures were measured for the flame with $\phi = 0.3$ and $x_{O_3} = 2.0$ mol%, and for the flame with $\phi = 0.5$ and $x_{O_3} = 1.6$ mol%, i.e., 865 and 860 K, respectively, which is within the reported uncertainty. It has been

previously demonstrated experimentally that the addition of ozone plays a great role in the maximal temperature reached in such flames [30], which can explain that the ultra-lean flame does not show a lower maximal temperature as the ozone concentration is higher in this flame. The temperatures for flames doped with OME-2 are slightly lower than the maximal temperature of the ozone-seeded DME/O₂ cool flame in same conditions (equivalence ratio of $\phi = 0.3$ and $x_{O_3} = 2.0$ mol%), which amounted to 884 K [30]. The position of the cool flame front, as visible from the steep increase of the temperature, is overpredicted by the model. The maximal temperature of the cool flames and the decrease of temperature, as the gases are cooled down in the vicinity of the stagnation plate, are predicted within the experimental uncertainty.

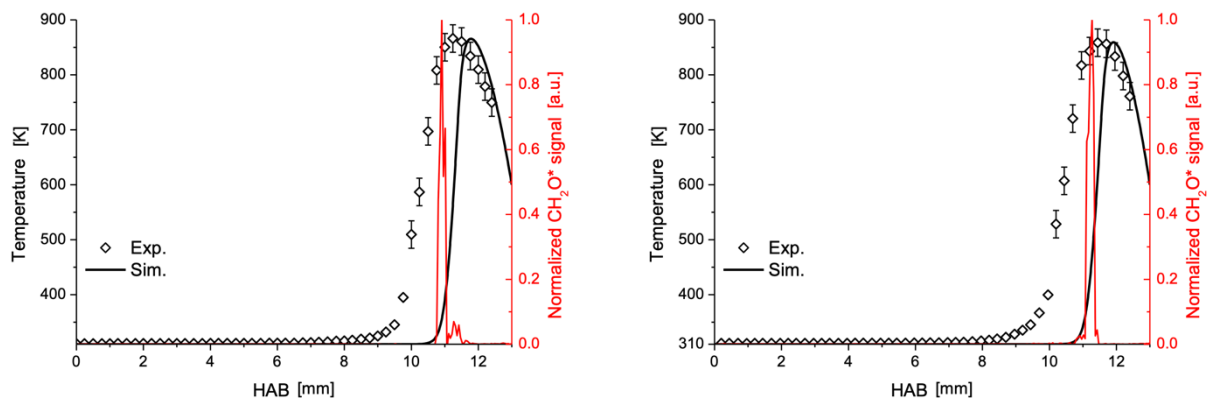


Fig. 6. Experimental (dots) and model simulated (full lines) temperature profiles of the stabilized, ozone-seeded OME-2/DME/O₂ premixed cool flames for equivalence ratios of $\phi = 0.3$ (left, $x_{O_3} = 2.0$ mol%) and $\phi = 0.5$ (right, $x_{O_3} = 1.6$ mol%). The normalized excited formaldehyde chemiluminescence signal is depicted by a red full line.

The measured mole fraction profiles of quantified intermediates and products as a function of the HAB in the cool flames are depicted in **Fig. 7** and **Fig. 8** for $\phi = 0.3$ with $x_{O_3} = 2.0$ mol% and $\phi = 0.5$ with $x_{O_3} = 1.6$ mol%, respectively, along with the simulation results and the CH₂O* chemiluminescence signal to indicate the position of the cool flame front. From our earlier studies [30, 31], it was shown that sampling in the pre-flame region is perturbed by the presence of ozone due to premature reactivity inside the sampling capillary. However, these

works have demonstrated that only the pre-flame region measurements are affected and this effect is negligible once ozone has decomposed in the cool flame. Therefore, the region downstream the flame front can be considered to validate kinetic models. The experimental measurements that are likely to be perturbed by the in-capillary reactivity are depicted in grey in **Fig. 7** and **Fig. 8**. The discussion will therefore be limited to the post-flame region, which is situated at HABs of about 11 mm and higher.

In this study, the major interest is in the decomposition of OME-2 and characteristic reaction products, such as methoxymethyl formate. It is observed that in all cases, except for ozone, the mole fraction profiles evolve toward a steady concentration downstream the cool flame, which indicates that at this position decomposition has stopped. The conversion of fuels is limited to about 30 and 50% in the case of DME, and 40 and 55% in the case of OME-2, with the highest conversions observed for the ultra-lean cool flame ($\phi = 0.3$). From these observations, it follows that OME-2 is the most reactive compound in the fuel feed. The DME and OME-2 conversions are well predicted by the developed kinetic model, although the mole fraction of OME-2 downstream the flame front is slightly underpredicted for both cool flames. This partial conversion of the fuels is a characteristic of cool flames. The concentrations of molecular oxygen and ozone are predicted by the model within the experimental uncertainty margins. Full conversion was measured for ozone, while the conversion of molecular oxygen remained marginal. The other detected reaction products were formaldehyde, methanol, CO, CO₂, methyl formate, OME-1 and methoxymethyl formate. The formation of molecules with carbon-carbon bonds requires recombination of carbon radicals since carbon-carbon bonds are not present in the fuels. However, carbon radicals will more easily recombine with abundantly present molecular and atomic oxygen, which explains why species consisting of solely carbon and hydrogen atoms, i.e., hydrocarbons, were not detected. Of interest is the methoxymethyl

formate product as it is a direct decomposition product of OME-2 cool flames and is not observed in similar DME flames [30]. The concentration in the post-flame region is underpredicted, by 20 % and 15 % for the ultra-lean and lean cool flame, respectively. The major reaction products were formaldehyde and CO, which are very well predicted. Methyl formate shows the largest discrepancy between experimental and model predicted mole fractions, with an observed deviation of a factor two. There are no significant differences observed in the relative importance of the different reaction products between both cool flames. However, it is remarkable that the kinetic model results are slightly less accurate in the case of the ultra-lean cool flame. A possible explanation could be that an increase of the ozone feed leads to more atomic oxygen in the cool flame, while the included number of reactions between atomic oxygen and fuel in the model is limited and the associated kinetic parameters are mostly based upon analogies instead of first principles. The predicted mole fraction profiles as a function of the HAB for other minor species (methanol, CO₂ and DMM/OME-1) can be found in the Supplementary Material (Fig. S7 and Fig. S8). We tried to simulate the cool flames with the model of Cai et al. [19] but for both conditions there was no cool flame observed, which is likely related to issues with the DME chemistry in the model.

5.3.2. Rate of production analysis

A reaction pathway analysis was performed for the OME-2/DME/O₂ cool flame with equivalence ratio $\phi = 0.3$ and $x_{O_3} = 2.0$ mol% to investigate the low-temperature chemistry of OME-2 with more detail. The results are depicted in **Fig. 9**. For a comprehensive reading of the figure, only the reaction pathways corresponding with a significant flux are shown. The analysis was realized for two different conditions in the cool flame, the first one is at the position where the cool flame temperature amounts to 450 K (underlined values) and the second one where the

cool flame temperature amounts to 600 K (bold values). These temperatures correspond with OME-2 conversions of 3 and 14 %, respectively, and were chosen, in the first case to better capture the reactions responsible for the first stage of ignition of the fuel, and in the second case to highlight the reactions related to the low-temperature conversions of the fuels in such conditions. It is relevant only in the presence of ozone, as this initiates the reactivity at lower temperatures than usual. The observed and quantified species during the experiments are encircled in red in **Fig. 9**. The interested reader is referred to the study by Panaget et al. [30] for details about the decomposition chemistry of DME in stabilized, ozone-assisted cool flames.

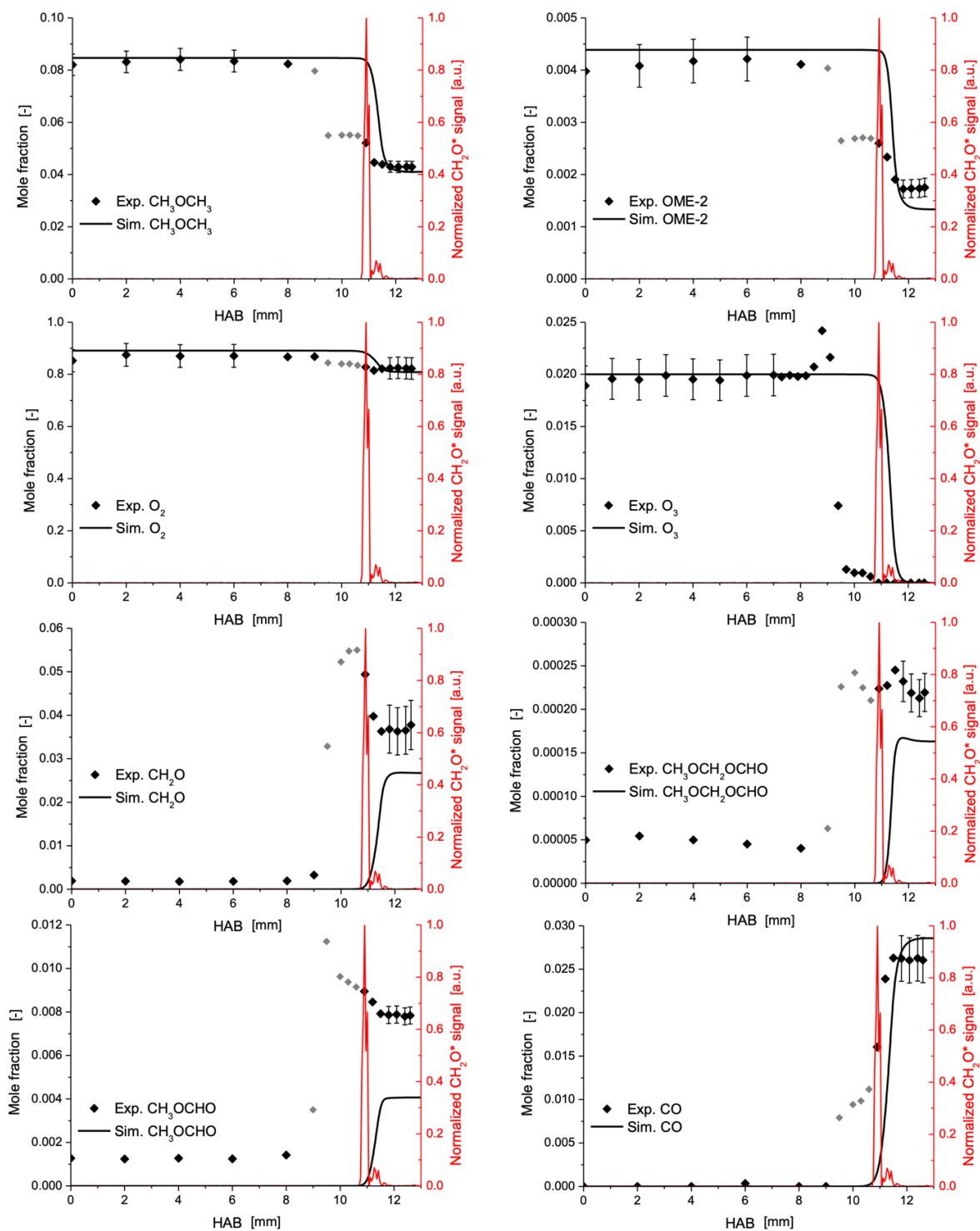


Fig. 7. Species mole fraction profiles (DME, OME-2, molecular oxygen, ozone, formaldehyde, methoxymethyl formate, methyl formate and CO) as function of HAB for the $\phi = 0.3$, $x_{O_3} = 2.0$ mol% stabilized premixed cool flame (fuel: 5.0 mol% OME-2, 95.0 mol% DME). Grey symbols represent the area of the flame perturbed by in-capillary reactivity. The normalized excited formaldehyde chemiluminescence signal is depicted by a red full line.

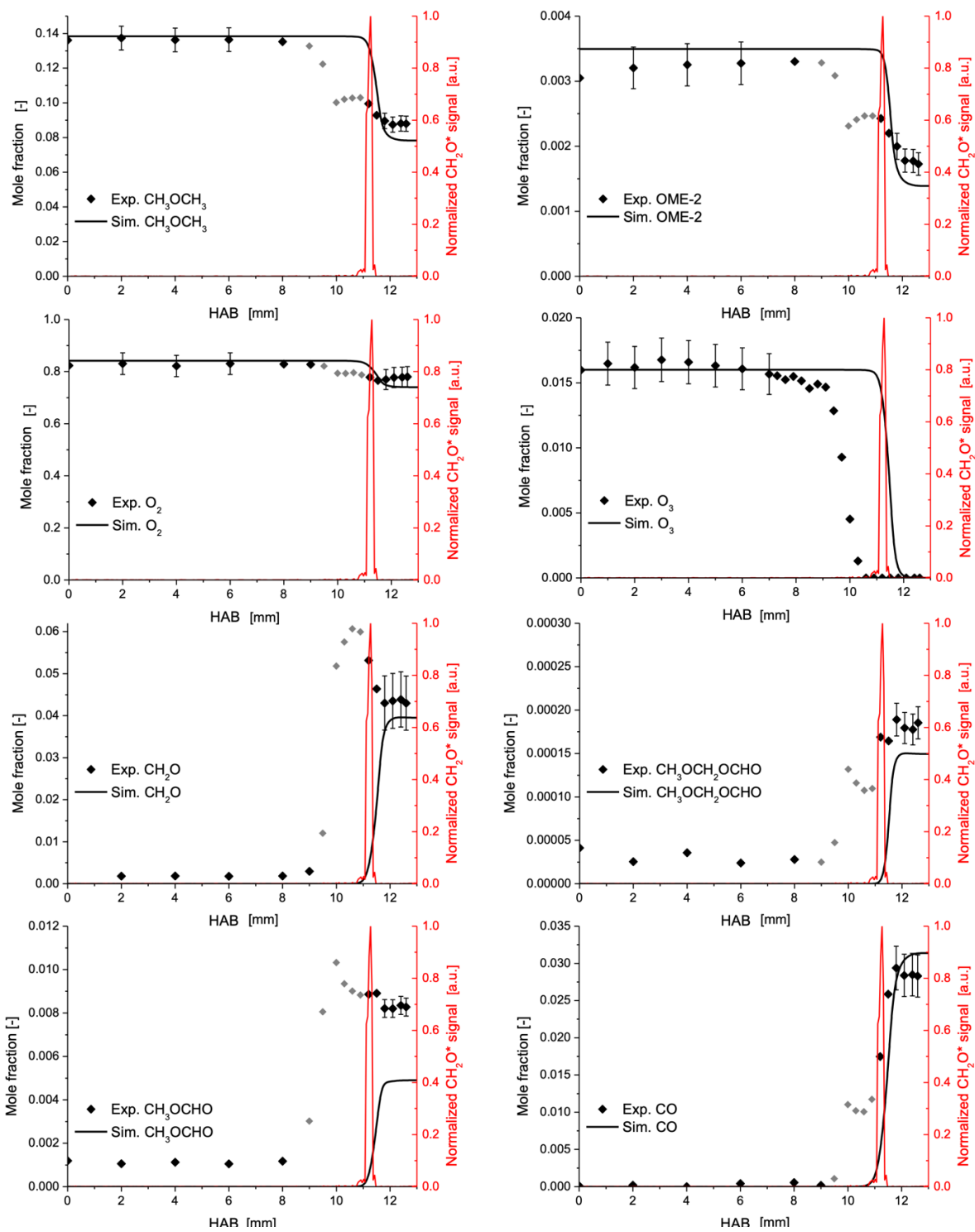


Fig. 8. Species mole fraction profiles (DME, OME-2, molecular oxygen, ozone, formaldehyde, methoxymethyl formate, methyl formate and CO) as function of HAB for the $\phi = 0.5$, $x_{O_3} = 1.6$ mol% stabilized premixed cool flame (fuel: 2.5 mol% OME-2, 97.5 mol% DME). Grey symbols represent the area of the flame perturbed by in-capillary reactivity. The normalized excited formaldehyde chemiluminescence signal is depicted by a red full line.

Unimolecular decomposition of ozone occurs at low temperatures due to the unstable nature of this molecule and results in the formation of atomic oxygen ($O\cdot$) and molecular oxygen. Atomic oxygen can react with DME and OME-2 by hydrogen abstraction reactions to form the hydroxyl radical and fuel radicals, i.e., $R_1\cdot$ and $R_2\cdot$ in the case of OME-2. Moreover, atomic oxygen can recombine with radicals to form species with an oxy functionality. Hydrogen abstractions by molecular oxygen are a negligible contribution to the initiation of the low-temperature chemistry under the given reaction conditions. Because of their formation from atomic oxygen, reactive hydroxyl radicals are abundantly present and dominate the hydrogen abstractions of OME-2. At 600 K, a small fraction of OME-2, i.e., 1 %, also reacts via hydrogen abstraction from the hydroperoxyl radical to form hydroperoxide. The secondary carbon radical of OME-2 is formed in larger proportions than the primary radical for both temperatures. After hydrogen abstraction, the formed fuel radical can add onto molecular oxygen. In the case of $R_1OO\cdot$, the species will mainly isomerize via intramolecular hydrogen abstraction to form $\cdot Q_{1,3}OOH$, and subsequently decomposes via β -scission to form methyl formate and $\cdot CH_2OCH_2OOH$. Only 3 % of the $\cdot Q_{1,3}OOH$ adds to molecular oxygen at the condition of 3 % OME-2 conversion. This addition no longer proceeds at the condition of 14 % OME-2 conversion, i.e., at increased temperatures. The second most important decomposition pathway of $R_1OO\cdot$ is isomerization into $\cdot Q_{1,2}OOH$ followed by β -scission to form a keto hydroperoxide and the methoxymethyl radical. The formation of $\cdot Q_{1,3}OOH$ is favored over $\cdot Q_{1,2}OOH$ since the associated intramolecular hydrogen abstraction has the lowest activated transition state, being about 10 kJ mol^{-1} more stable. This difference has a big influence at low temperatures, even though $\cdot Q_{1,3}OOH$ is formed via an eight-membered cyclic transition state and $\cdot Q_{1,2}OOH$ is formed via a six-membered cyclic transition state. At higher temperatures, i.e., at higher

OME-2 conversions, the fraction forming $\bullet Q_{1,2}OOH$ increases as the influence of the entropy becomes more important. The formation of $\bullet Q_{1,4}OOH$ via a ten-membered cyclic transition state is even higher activated and therefore does not contribute to the decomposition. For 3 % OME-2 conversion, some additional reactions proceed that are typical for atmospheric chemistry, which are not found to occur at 14 % conversion. Moreover, a small fraction of $R_1\bullet$ isomerizes into $R_2\bullet$ at higher temperatures. These observations can be explained by the increase in temperature with increased conversion, which enables more activated reactions, e.g., the intramolecular hydrogen abstraction of $R_1\bullet$ to $R_2\bullet$, to proceed. In the case of $R_2\bullet$, the chemistry is quite different for both investigated reaction conditions. A clear change is observed in the branching ratio for $R_2\bullet$ as an increase of the temperature from 450 to 600 K already leads to β -scissions to occur instead of the addition to molecular oxygen, i.e., only 42 % adds to molecular oxygen at 600 K compared to 99 % at 450 K. Two carbon-centered β -scission reactions are possible for $R_2\bullet$, i.e., one forming methoxymethyl formate and the methyl radical, and the more dominant one forming methyl formate and the methoxymethyl radical. The two aforementioned molecular species are both detected during the experiments. The β -scission of $R_2\bullet$ is the most important pathway to form methoxymethyl formate at the given reaction conditions. The decomposition of $R_2OO\bullet$ proceeds at 450 K partly via typical atmospheric chemistry but the major part, i.e., 67 %, isomerizes into $\bullet Q_{2,3}OOH$. At 600 K, practically all $R_2OO\bullet$ isomerizes via an intramolecular hydrogen abstraction into $\bullet Q_{2,3}OOH$. The latter molecule decomposes mainly via β -scission, especially at elevated temperatures, to form two methyl formate molecules. A fraction decomposes via cyclic ether formation to form the hydroxyl radical and a four-membered cyclic ether, which can decompose to form similarly two methyl formate molecules. At 450 K, 21% of $\bullet Q_{2,3}OOH$ adds to molecular oxygen to form $\bullet OOQ_{2,3}OOH$

accompanied with a shift of the hydrogen from a primary carbon to the peroxy functionality. This finding shows the importance of theoretical calculations as the production of a keto hydroperoxide is frequently the only reaction pathway considered during kinetic modeling while the formation of the alternative $\bullet\text{P}(\text{OOH})_2$ is considered as a minor contribution. The global low-temperature reactivity of the system can then be affected and the species distribution is mispredicted. The formed primary radical mainly decomposes via cyclic ether formation reactions to form both four- and six-membered rings. These cyclic ethers decompose via the previously discussed unimolecular decomposition pathways. However, it follows that the addition of hydroperoxy alkyl radicals to molecular oxygen is not a dominant pathway during the low-temperature oxidation chemistry, even under ultra-lean oxidation conditions. Via some atmospheric chemistry reactions, a radical is formed with an oxy functionality. These decompose mainly via β -scissions of the carbon-hydrogen bond to form a carbonyl functionality and the hydrogen atom, and not via hydrogen abstractions. Therefore, few species with hydroxyl functionalities are found in this rate of production analysis, which is also confirmed by the experimental observations. Also note that for both $\text{R}_1\text{OO}\bullet$ and $\text{R}_2\text{OO}\bullet$, a significant part, i.e., 7 and 16 %, respectively, reacts with the hydroperoxyl radical by a hydrogen abstraction to form the associated hydroperoxide species at 3 % OME-2 conversion. This reaction no longer contributes at 14 % conversion.

The results of the sensitivity analyses are presented and discussed in the Supplementary Material (Fig. S9 and Fig. S10).

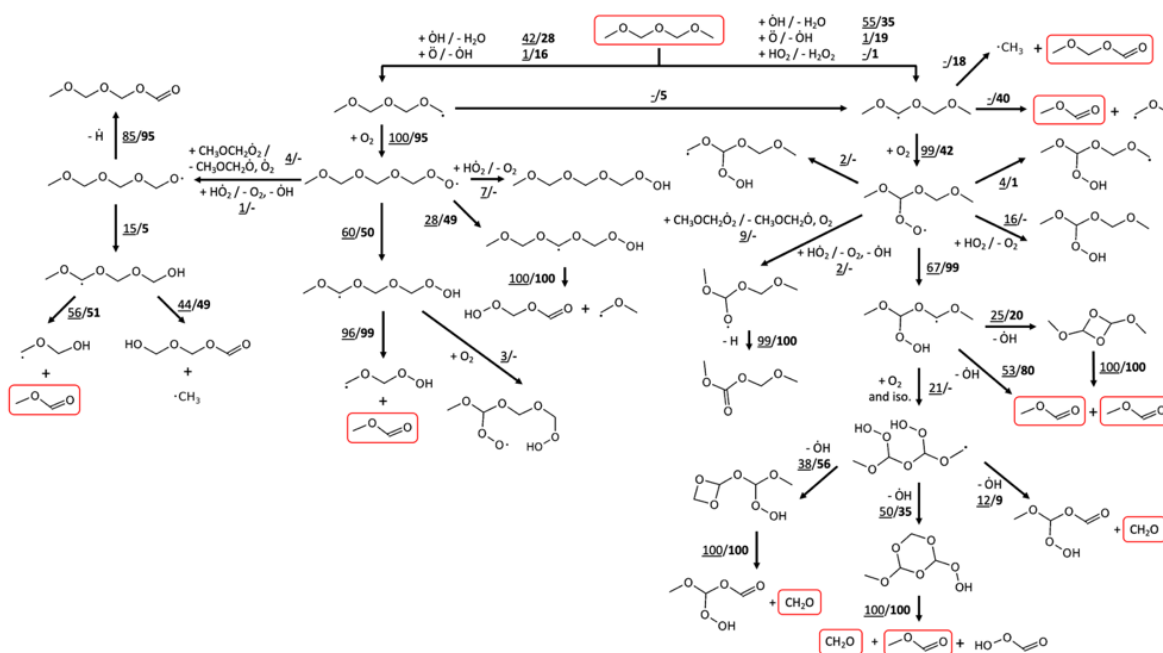


Fig. 9. Rate of production analysis with the newly developed kinetic model for a stabilized, ozone-assisted OME-2/DME/O₂ premixed cool flame with equivalence ratio $\phi = 0.3$ and $x_{O_3} = 2.0$ mol% at conditions of 3 (underlined) and 14 (bold) % conversion of OME-2 in the cool flame. Numbers represent normalized fluxes. Species encircled were experimentally observed and quantified.

5.4. Additional kinetic model validation

The newly developed kinetic model for OME-2 was additionally validated against experimental data from the literature for low-temperature oxidation conditions. IDT measurements from a RCM and ST were used as acquired in the studies of De Ras et al. [15] and Cai et al. [19], respectively. Moreover, validation against the RCM data from Drost et al. [20] is provided in the Supplementary Material (Fig. S12). Validation of the kinetic model against pyrolysis data was extensively performed in our previous studies [15, 17, 28] and is identical for this new model as the chemistry related to pyrolysis was not adapted.

5.4.1. Rapid compression machine measurements

The performance of the developed kinetic model to predict the measured first-stage (FSIDT) and total (IDT) IDTs of OME-2/air mixtures from the ULille RCM unit for an equivalence ratio ϕ of 0.5 and pressures of 0.5 and 1.0 MPa [15] is depicted in **Fig. 10**. The kinetic model can well reproduce the experimental observations as a function of the reaction temperature. Auto-ignition of OME-2 has a pronounced two-stage ignition, which is also predicted by the model simulation results. The increase in reactivity due to an increase of the compression pressure is well captured by the model. There is a slight overestimation of the predicted IDTs at higher temperatures for 0.5 MPa, however, the predicted IDTs at 1.0 MPa and FSIDTs completely agree with the experimental observations. At higher temperatures, the experimental results might be impacted by the compression phase as the IDTs are very short. The auto-ignition characteristics of several fuels have already been investigated with this experimental unit [61, 62] and when compared, it can be concluded that OME-2 is a very reactive fuel at low-temperature oxidation conditions. Compared to our earlier published OME-2 model [15], the simulated (total) IDTs have not changed significantly, however, the FSIDTs are slightly shifted and are now better in agreement with the experimental results. The observation that the IDTs have not changed significantly even though the addition of molecular oxygen to hydroperoxyl alkyl radicals has been added to the kinetic model is an indication of the rather low influence of these pathways on the prediction of the IDTs.

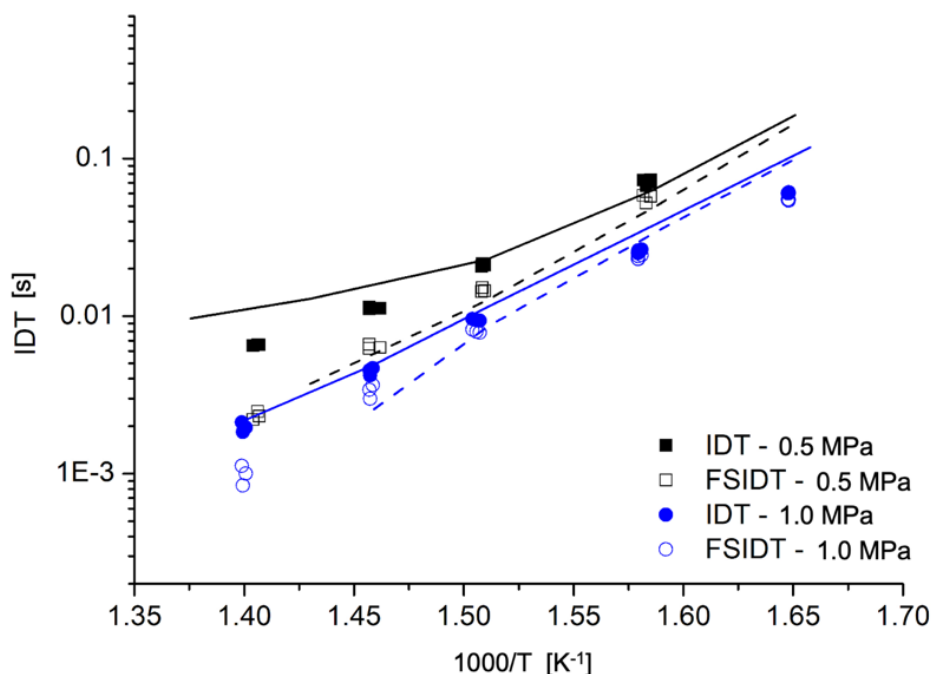


Fig. 10. Comparison between experimental first-stage (FSIDT) and total (IDT) ignition delay times (open and full points, respectively) from the ULille rapid compression machine (RCM) [15] and simulation results of FSIDT (dotted lines) and IDT (full lines) for OME-2/air mixtures with an equivalence ratio ϕ of 0.5 for pressures of 0.5 (black) and 1.0 MPa (blue) and temperatures ranging from 600 to 715 K.

A rate of production analysis is presented for these RCM experiments at 700 K to unravel the important decomposition pathways and to determine the actual influence of chain branching reactions on the reactivity of OME-2. In **Fig. 11**, the results for a pressure of 1.0 MPa and an equivalence ratio ϕ of 0.5 are depicted at the moment of 5 and 20 % fuel consumption. Only the reaction pathways representing a flux of more than 5 % are depicted. Initially, a hydrogen abstraction creates an OME-2 radical with the hydroxyl radical being the most dominant abstracting species, followed by the hydrogen atom. Other radicals, such as the methyl, hydroperoxyl, methyl peroxy and methoxy radicals, do not significantly contribute to the hydrogen abstractions from OME-2. The secondary carbon radical is formed in larger proportions by hydrogen abstractions, but also due to the isomerization of the primary radical

into the secondary radical. In the case of the primary radical, the major fraction of the radicals adds to molecular oxygen, isomerizes to a secondary alkyl radical and decomposes via β -scission reactions. The addition of the alkyl hydroperoxy species to molecular oxygen does not contribute to the decomposition at the given reaction conditions. Note that the methoxymethyl radical is formed by β -scission, which has an accelerating effect due to the low-temperature chemistry of DME. Only a small fraction of the primary radical of OME-2 decomposes directly via β -scission to form formaldehyde and the methoxymethoxymethyl radical. In the case of the secondary carbon radical, the results are somewhat different as the addition of molecular oxygen is less important compared to the β -scission reactions. The results for 5 and 20 % fuel consumption are very similar, except that in the case of the secondary radical the addition to molecular oxygen does not significantly contribute anymore at larger fuel consumptions. This was also observed from the rate of production analysis of the cool flame. The addition of hydroperoxy alkyl radicals of OME-2 to molecular oxygen is thus not contributing to the decomposition chemistry. However, in the case of DME, it is significantly contributing.

The results of the sensitivity analyses are presented and discussed in the Supplementary Material (Fig. S11).

visible in our previously developed model. Additionally, the observed reactivity plateau as function of temperature in the case of 2.0 MPa is reproduced by our developed model. On average, the newly developed model is able to predict the measured IDT within the experimental uncertainty margin. The comparison for different equivalence ratios is depicted in **Fig. 12 b**. The model is performing very accurately in the case of fuel-rich and stoichiometric conditions and describes the experimental trends well. Only for an equivalence ratio ϕ of 0.5, the model is underpredicting the IDTs in the low-temperature range, and as such there is an overprediction of the reactivity compared to the experimental data. However, this overprediction is reduced compared to our previous model version, although the chain branching reactions that increase the reactivity have been added. This is another indication that the chain branching reactions are not significantly contributing to the decomposition chemistry for OME-2, even for high oxygen concentrations, i.e., low equivalence ratios.

A rate of production analysis and sensitivity analysis were not performed as the results would be very similar to the results discussed before for the RCM experiments, i.e., the same chemistry proceeds.

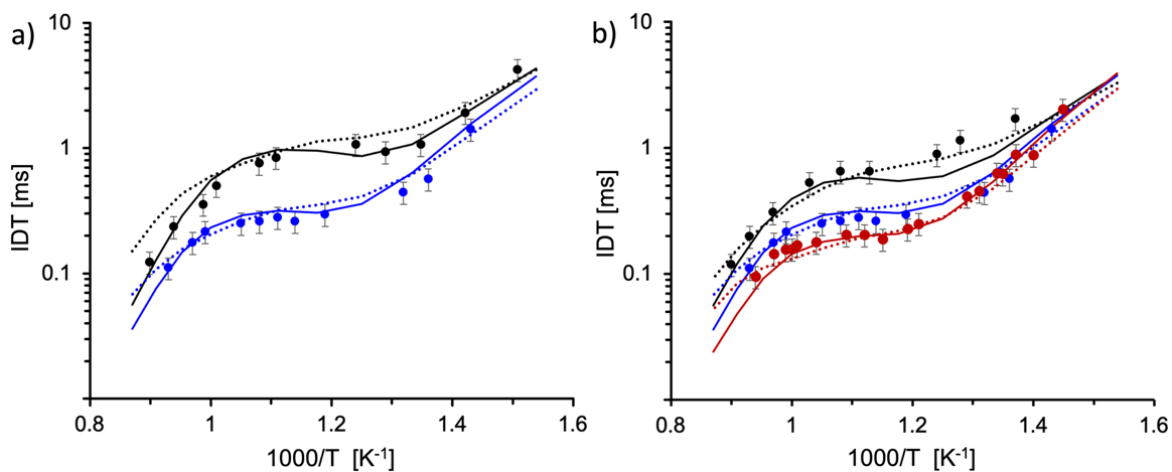


Fig. 12. Comparison between experimental ignition delay times (IDT, points) from a shock tube apparatus for OME-2/air mixtures [19] and simulation results with the model of Cai et al. [19]

(dotted lines) and the new kinetic model from this study (full lines). a) Results for an equivalence ratio ϕ of 1.0 with a pressure of 1.0 MPa (black) and 2.0 MPa (blue). b) Results for a compression pressure of 2.0 MPa and equivalence ratios of 0.5 (black), 1.0 (blue) and 2.0 (red).

6. Conclusions and future work

In this study, the low-temperature oxidation chemistry of OME-2 was studied in more detail by means of newly acquired experimental data and a newly developed kinetic model. Stabilized, ozone-seeded cool flame experiments were performed with OME-2/DME/O₂ premixed flames in a heated stagnation plate burner for different fuel-lean equivalence ratios. The detected and quantified reaction products were formaldehyde, CO, CO₂, methanol, methyl formate and methoxymethyl formate. Quantum chemical calculations have been performed for the first time for the different hydroperoxy alkyl peroxy radicals of OME-2 to investigate their decomposition pathways. It was observed that strong intramolecular interactions, i.e., hydrogen bonds, are present within these compounds, which dominate the thermodynamic properties and make it difficult to calculate these properties with group additivity schemes. A new kinetic model has been developed for the pyrolysis and oxidation of OME-2 based on first principles with detailed low-temperature chemistry included. The model is able to predict the experimental observations of the cool flames and additional IDTs from literature satisfactorily and on average performs within the experimental accuracy margins without adjustment of reaction rate coefficients or thermodynamic parameters. The addition of hydroperoxy alkyl radicals to molecular oxygen to form hydroperoxy alkyl peroxy radicals was found to not significantly affect the prediction of the OME-2 IDTs, even when experiments at fuel-lean reaction conditions were investigated. It is the low-temperature oxidation chemistry of DME that plays an important role in the high reactivity of OME-2. When DME is not part of the feed,

its radicals are also formed as intermediates during OME-2 decomposition. The new fundamental knowledge obtained for OME-2 can now be extrapolated to develop detailed kinetic models for the pyrolysis and oxidation of larger OMEs of interest, i.e., OME-3, OME-4 and OME-5. In addition, this new detailed model will be helpful in the development of more concise models, which describe the radical decomposition of OMEs, to be used in the case of computationally intensive applications.

Supplementary Material

A main Word document (.docx) is available, which contains the measured temperature profiles of the cool flames along the axis from bottom to top and vice versa, additional figures of lowest-energy conformers, additional potential energy surfaces with discussion, additional figures with experimental results, results of the sensitivity analyses, and validation of the kinetic model against rapid compression machine experiments from Drost et al. [20]. This main document also outlines the content of the additional files and their designations, which are the experimental results from the stabilized, ozone-seeded OME-2/DME/O₂ premixed cool flames in the heated stagnation plate burner in a separate Excel file (.xlsx), a second Word document (.docx) containing the quantum chemical results, the developed kinetic model for OME-2 in CHEMKIN format (.inp) and an input file (.inp) with the transport properties of the species in CHEMKIN format.

Declaration of Competing Interest

The authors declare that they have no known competing financial interests or personal relationships that could have appeared to influence the results reported in this paper.

Acknowledgements

This work was established in a joint call to strengthen collaboration between I-SITE Université Lille Nord-Europe (members and national partners) and Ghent University. The computational resources and services used in this work were provided by the VSC (Flemish Supercomputer Center), funded by the Fund for scientific Research Flanders (FWO) and the Flemish Government department EWI. Kevin De Ras and Jeroen Aerssens acknowledge the Fund for Scientific Research Flanders (FWO) for financial support via doctoral fellowship grants 3F018119 and 1S17922N, respectively. The research leading to these results has also received funding from the European Research Council under the European Union's Horizon 2020 research and innovation programme / ERC grant agreement n° 818607. This work is a contribution to the LabEx CaPPA project funded by the French National Agency under contract « ANR-11-LABX-0005-01 », the CPER research project ECRIN funded by the French Ministère de l'Enseignement Supérieur et de la Recherche. The authors thank the Regional Council « Hauts-de-France » and the « European Regional Development Fund » for their financial support to these projects.

References

- [1] K.M. Van Geem, B.M. Weckhuysen, Toward an e-chemistree: Materials for electrification of the chemical industry, *MRS Bulletin* 46 (2021) 1187-1196.
- [2] L.S. Tran, B. Sirjean, P.-A. Glaude, R. Fournet, F. Battin-Leclerc, Progress in detailed kinetic modeling of the combustion of oxygenated components of biofuels, *Energy* 43 (2012) 4-18.
- [3] S. Deutz, D. Bongartz, B. Heuser, A. Kätelhön, L. Schulze Langenhorst, A. Omari, M. Walters, J. Klankermayer, W. Leitner, A. Mitsos, S. Pischinger, A. Bardow, Cleaner production of cleaner fuels: wind-to-wheel – environmental assessment of CO₂-based oxymethylene ether as a drop-in fuel, *Energy & Environmental Science* 11 (2018) 331-343.
- [4] K. De Ras, R. Van de Vijver, V.V. Galvita, G.B. Marin, K.M. Van Geem, Carbon capture and utilization in the steel industry: challenges and opportunities for chemical engineering, *Current Opinion in Chemical Engineering* 26 (2019) 81-87.
- [5] D. Bongartz, J. Burre, A. Mitsos, Production of Oxymethylene Dimethyl Ethers from Hydrogen and Carbon Dioxide—Part I: Modeling and Analysis for OME1, *Industrial & Engineering Chemistry Research* 58 (2019) 4881-4889.
- [6] A. Omari, B. Heuser, S. Pischinger, C. Rüdinger, Potential of long-chain oxymethylene ether and oxymethylene ether-diesel blends for ultra-low emission engines, *Applied Energy* 239 (2019) 1242-1249.
- [7] J. Liu, H. Wang, Y. Li, Z. Zheng, Z. Xue, H. Shang, M. Yao, Effects of diesel/PODE (polyoxymethylene dimethyl ethers) blends on combustion and emission characteristics in a heavy duty diesel engine, *Fuel* 177 (2016) 206-216.
- [8] Z. Wang, H. Liu, J. Zhang, J. Wang, S. Shuai, Performance, Combustion and Emission Characteristics of a Diesel Engine Fueled with Polyoxymethylene Dimethyl Ethers (PODE3-4)/ Diesel Blends, *Energy Procedia* 75 (2015) 2337-2344.
- [9] H. Liu, X. Wang, Y. Wu, X. Zhang, C. Jin, Z. Zheng, Effect of diesel/PODE/ethanol blends on combustion and emissions of a heavy duty diesel engine, *Fuel* 257 (2019) 116064.
- [10] B. Lumpp, D. Rothe, C. Pastötter, R. Lämmermann, E. Jacob, Oxymethylene Ethers as Diesel Fuel Additives of the Future, *MTZ worldwide eMagazine* 72 (2011) 34-38.
- [11] D. Pélerin, K. Gaukel, M. Härtl, E. Jacob, G. Wachtmeister, Potentials to simplify the engine system using the alternative diesel fuels oxymethylene ether OME1 and OME3–6 on a heavy-duty engine, *Fuel* 259 (2020) 116231.
- [12] K. Vertin, J. Ohi, D. Naegeli, K. Childress, G. Hagen, C. McCarthy, A.S. Cheng, R. Dibble, Methylal and Methylal-Diesel Blended Fuels from Use In Compression-Ignition Engines, 1999.
- [13] J. Burger, M. Siegert, E. Ströfer, H. Hasse, Poly(oxymethylene) dimethyl ethers as components of tailored diesel fuel: Properties, synthesis and purification concepts, *Fuel* 89 (2010) 3315-3319.
- [14] A.K. Agarwal, A.P. Singh, A. García, J. Monsalve-Serrano, Challenges and Opportunities for Application of Reactivity-Controlled Compression Ignition

- Combustion in Commercially Viable Transport Engines, *Progress in Energy and Combustion Science* 93 (2022) 101028.
- [15] K. De Ras, M. Kusenbergh, G. Vanhove, Y. Fenard, A. Eschenbacher, R.J. Varghese, J. Aerssens, R. Van de Vijver, L.-S. Tran, J.W. Thybaut, K.M. Van Geem, A detailed experimental and kinetic modeling study on pyrolysis and oxidation of oxymethylene ether-2 (OME-2), *Combustion and Flame* 238 (2022) 111914.
- [16] B. Li, Y. Li, H. Liu, F. Liu, Z. Wang, J. Wang, Combustion and emission characteristics of diesel engine fueled with biodiesel/PODE blends, *Applied Energy* 206 (2017) 425-431.
- [17] K. De Ras, M. Kusenbergh, J.W. Thybaut, K.M. Van Geem, Unraveling the carbene chemistry of oxymethylene ethers: Experimental investigation and kinetic modeling of the high-temperature pyrolysis of OME-2, *Proceedings of the Combustion Institute*, doi:[https://doi.org/10.1016/j.proci.2022.07.069\(2022\)](https://doi.org/10.1016/j.proci.2022.07.069(2022)).
- [18] X. Zhong, H. Wang, Q. Zuo, Z. Zheng, J. Wang, W. Yin, M. Yao, Experimental and kinetic modeling studies of polyoxymethylene dimethyl ether (PODE) pyrolysis in jet stirred reactor, *Journal of Analytical and Applied Pyrolysis* 159 (2021) 105332.
- [19] L. Cai, S. Jacobs, R. Langer, F. vom Lehn, K.A. Heufer, H. Pitsch, Auto-ignition of oxymethylene ethers (OMEn, n = 2–4) as promising synthetic e-fuels from renewable electricity: shock tube experiments and automatic mechanism generation, *Fuel* 264 (2020) 116711.
- [20] S. Drost, R. Schießl, M. Werler, J. Sommerer, U. Maas, Ignition delay times of polyoxymethylene dimethyl ether fuels (OME2 and OME3) and air: Measurements in a rapid compression machine, *Fuel* 258 (2019) 116070.
- [21] S. Eckart, L. Cai, C. Fritsche, F. vom Lehn, H. Pitsch, H. Krause, Laminar burning velocities, CO, and NO_x emissions of premixed polyoxymethylene dimethyl ether flames, *Fuel* 293 (2021) 120321.
- [22] J.M. Ngugi, S. Richter, M. Braun-Unkhoff, C. Naumann, M. Köhler, U. Riedel, A Study on Fundamental Combustion Properties of Oxymethylene Ether-2, *Journal of Engineering for Gas Turbines and Power* 144 (2021).
- [23] H. Wang, Z. Yao, X. Zhong, Q. Zuo, Z. Zheng, Y. Chen, M. Yao, Experimental and kinetic modeling studies on low-temperature oxidation of Polyoxymethylene Dimethyl Ether (DMM1-3) in a jet-stirred reactor, *Combustion and Flame* 245 (2022) 112332.
- [24] Y. Fenard, G. Vanhove, A Mini-Review on the Advances in the Kinetic Understanding of the Combustion of Linear and Cyclic Oxymethylene Ethers, *Energy & Fuels* 35 (2021) 14325-14342.
- [25] T. He, Z. Wang, X. You, H. Liu, Y. Wang, X. Li, X. He, A chemical kinetic mechanism for the low- and intermediate-temperature combustion of Polyoxymethylene Dimethyl Ether 3 (PODE3), *Fuel* 212 (2018) 223-235.
- [26] W. Sun, G. Wang, S. Li, R. Zhang, B. Yang, J. Yang, Y. Li, C.K. Westbrook, C.K. Law, Speciation and the laminar burning velocities of poly(oxymethylene) dimethyl ether 3 (POMDME3) flames: An experimental and modeling study, *Proc. Combust. Inst.* 36 (2017) 1269-1278.
- [27] Y. Zhao, N. Li, Y. Xie, Y. Cheng, X. Wang, Study on chemical kinetic mechanisms of Polyoxymethylene Dimethyl Ethers (PODEn), *IOP Conference Series: Materials Science and Engineering* 768 (2020) 022056.

- [28] K. De Ras, M. Bonheure, J.W. Thybaut, K.M. Van Geem, The secondary chemistry of synthetic fuel oxymethylene ethers unraveled: Theoretical and kinetic modeling of methoxymethyl formate and formic anhydride decomposition, *Journal of the Energy Institute* 104 (2022) 46-54.
- [29] N.M. Vandewiele, K.M. Van Geem, M.-F. Reyniers, G.B. Marin, Genesys: Kinetic model construction using chemo-informatics, *Chemical Engineering Journal* 207-208 (2012) 526-538.
- [30] T. Panaget, N. Mokrani, S. Batut, A. Lahccen, Y. Fenard, L. Pillier, G. Vanhove, Insight into the Ozone-Assisted Low-Temperature Combustion of Dimethyl Ether by Means of Stabilized Cool Flames, *The Journal of Physical Chemistry A* 125 (2021) 9167-9179.
- [31] T. Panaget, K. Potier, S. Batut, A. Lahccen, Y. Fenard, L. Pillier, G. Vanhove, How ozone affects the product distribution inside cool flames of diethyl ether, *Proceedings of the Combustion Institute*, doi:[https://doi.org/10.1016/j.proci.2022.08.081\(2022\)](https://doi.org/10.1016/j.proci.2022.08.081(2022)).
- [32] M.V. Heitor, A.L.N. Moreira, Thermocouples and sample probes for combustion studies, *Progress in Energy and Combustion Science* 19 (1993) 259-278.
- [33] N. Lamoureux, P. Desgroux, A. El Bakali, J.F. Pauwels, Experimental and numerical study of the role of NCN in prompt-NO formation in low-pressure CH₄-O₂-N₂ and C₂H₂-O₂-N₂ flames, *Combustion and Flame* 157 (2010) 1929-1941.
- [34] J.T. Scanlon, D.E. Willis, Calculation of Flame Ionization Detector Relative Response Factors Using the Effective Carbon Number Concept, *Journal of Chromatographic Science* 23 (1985) 333-340.
- [35] J.A.M. Jr., M.J. Frisch, J.W. Ochterski, G.A. Petersson, A complete basis set model chemistry. VI. Use of density functional geometries and frequencies, *The Journal of Chemical Physics* 110 (1999) 2822-2827.
- [36] M.J. Frisch, G.W. Trucks, H.B. Schlegel, G.E. Scuseria, M.A. Robb, J.R. Cheeseman, G. Scalmani, V. Barone, G.A. Petersson, H. Nakatsuji, X. Li, M. Caricato, A.V. Marenich, J. Bloino, B.G. Janesko, R. Gomperts, B. Mennucci, H.P. Hratchian, J.V. Ortiz, A.F. Izmaylov, J.L. Sonnenberg, Williams, F. Ding, F. Lipparini, F. Egidi, J. Goings, B. Peng, A. Petrone, T. Henderson, D. Ranasinghe, V.G. Zakrzewski, J. Gao, N. Rega, G. Zheng, W. Liang, M. Hada, M. Ehara, K. Toyota, R. Fukuda, J. Hasegawa, M. Ishida, T. Nakajima, Y. Honda, O. Kitao, H. Nakai, T. Vreven, K. Throssell, J.A. Montgomery Jr., J.E. Peralta, F. Ogliaro, M.J. Bearpark, J.J. Heyd, E.N. Brothers, K.N. Kudin, V.N. Staroverov, T.A. Keith, R. Kobayashi, J. Normand, K. Raghavachari, A.P. Rendell, J.C. Burant, S.S. Iyengar, J. Tomasi, M. Cossi, J.M. Millam, M. Klene, C. Adamo, R. Cammi, J.W. Ochterski, R.L. Martin, K. Morokuma, O. Farkas, J.B. Foresman, D.J. Fox, *Gaussian 16 Rev. C.01*, Wallingford, CT, 2016.
- [37] R. Van de Vijver, K.M. Van Geem, G.B. Marin, On-the-fly ab initio calculations toward accurate rate coefficients, *Proceedings of the Combustion Institute* 37 (2019) 283-290.
- [38] A.L.L. East, L. Radom, Ab initio statistical thermodynamical models for the computation of third-law entropies, *The Journal of Chemical Physics* 106 (1997) 6655-6674.

- [39] L.A. Curtiss, K. Raghavachari, P.C. Redfern, J.A. Pople, Assessment of Gaussian-2 and density functional theories for the computation of enthalpies of formation, *The Journal of Chemical Physics* 106 (1997) 1063-1079.
- [40] G.A. Petersson, D.K. Malick, W.G. Wilson, J.W. Ochterski, J.A.M. Jr., M.J. Frisch, Calibration and comparison of the Gaussian-2, complete basis set, and density functional methods for computational thermochemistry, *The Journal of Chemical Physics* 109 (1998) 10570-10579.
- [41] C.A.R. Pappijn, F.H. Vermeire, R. Van de Vijver, M.-F. Reyniers, G.B. Marin, K.M. Van Geem, Bond additivity corrections for CBS-QB3 calculated standard enthalpies of formation of H, C, O, N, and S containing species, *International Journal of Chemical Kinetics* 53 (2021) 345-355.
- [42] C. Eckart, The Penetration of a Potential Barrier by Electrons, *Physical Review* 35 (1930) 1303-1309.
- [43] P.D. Paraskevas, M.K. Sabbe, M.-F. Reyniers, N. Papayannakos, G.B. Marin, Group Additive Values for the Gas-Phase Standard Enthalpy of Formation, Entropy and Heat Capacity of Oxygenates, *Chemistry – A European Journal* 19 (2013) 16431-16452.
- [44] H.-H. Carstensen, A.M. Dean, Rate Constant Rules for the Automated Generation of Gas-Phase Reaction Mechanisms, *The Journal of Physical Chemistry A* 113 (2009) 367-380.
- [45] H.-H. Carstensen, A.M. Dean, A quantitative kinetic analysis of CO elimination from phenoxy radicals, *International Journal of Chemical Kinetics* 44 (2012) 75-89.
- [46] A.G. Vandeputte, M.K. Sabbe, M.-F. Reyniers, V. Van Speybroeck, M. Waroquier, G.B. Marin, Theoretical Study of the Thermodynamics and Kinetics of Hydrogen Abstractions from Hydrocarbons, *The Journal of Physical Chemistry A* 111 (2007) 11771-11786.
- [47] S.W. Benson, J.H. Buss, Additivity Rules for the Estimation of Molecular Properties. Thermodynamic Properties, *The Journal of Chemical Physics* 29 (1958) 546-572.
- [48] M. Saeys, M.-F. Reyniers, G.B. Marin, V. Van Speybroeck, M. Waroquier, Ab initio group contribution method for activation energies for radical additions, *AIChE Journal* 50 (2004) 426-444.
- [49] P.D. Paraskevas, M.K. Sabbe, M.-F. Reyniers, N.G. Papayannakos, G.B. Marin, Group Additive Kinetics for Hydrogen Transfer Between Oxygenates, *The Journal of Physical Chemistry A* 119 (2015) 6961-6980.
- [50] L. Cai, H. Pitsch, S.Y. Mohamed, V. Raman, J. Bugler, H. Curran, S.M. Sarathy, Optimized reaction mechanism rate rules for ignition of normal alkanes, *Combust. Flame* 173 (2016) 468-482.
- [51] J. Bugler, K.P. Somers, E.J. Silke, H.J. Curran, Revisiting the Kinetics and Thermodynamics of the Low-Temperature Oxidation Pathways of Alkanes: A Case Study of the Three Pentane Isomers, *The Journal of Physical Chemistry A* 119 (2015) 7510-7527.
- [52] W.K. Metcalfe, S.M. Burke, S.S. Ahmed, H.J. Curran, A Hierarchical and Comparative Kinetic Modeling Study of C1 – C2 Hydrocarbon and Oxygenated Fuels, *International Journal of Chemical Kinetics* 45 (2013) 638-675.

- [53] J. Aerssens, F. Vermeire, S.U. Aravindakshan, R. Van de Vijver, Kevin M. Van Geem, The merit of pressure dependent kinetic modelling in steam cracking, *Faraday Discussions* 238 (2022) 491-511.
- [54] C.-W. Zhou, Y. Li, U. Burke, C. Banyon, K.P. Somers, S. Ding, S. Khan, J.W. Hargis, T. Sikes, O. Mathieu, E.L. Petersen, M. AlAbbad, A. Farooq, Y. Pan, Y. Zhang, Z. Huang, J. Lopez, Z. Loparo, S.S. Vasu, H.J. Curran, An experimental and chemical kinetic modeling study of 1,3-butadiene combustion: Ignition delay time and laminar flame speed measurements, *Combustion and Flame* 197 (2018) 423-438.
- [55] M. Baigmohammadi, V. Patel, S. Martinez, S. Panigrahy, A. Ramalingam, U. Burke, K.P. Somers, K.A. Heufer, A. Pekalski, H.J. Curran, A Comprehensive Experimental and Simulation Study of Ignition Delay Time Characteristics of Single Fuel C1–C2 Hydrocarbons over a Wide Range of Temperatures, Pressures, Equivalence Ratios, and Dilutions, *Energy & Fuels* 34 (2020) 3755-3771.
- [56] Y. Wu, S. Panigrahy, A.B. Sahu, C. Bariki, J. Beeckmann, J. Liang, A.A.E. Mohamed, S. Dong, C. Tang, H. Pitsch, Z. Huang, H.J. Curran, Understanding the antagonistic effect of methanol as a component in surrogate fuel models: A case study of methanol/n-heptane mixtures, *Combustion and Flame* 226 (2021) 229-242.
- [57] F. Battin-Leclerc, J.M. Simmie, E. Blurock, Cleaner combustion, *Developing Detailed Chemical Kinetic Models. Series: Green Energy and Technology*. Cham: Springer International Publishing AG, (2013).
- [58] M.K. Sabbe, M. Saeys, M.-F. Reyniers, G.B. Marin, V. Van Speybroeck, M. Waroquier, Group Additive Values for the Gas Phase Standard Enthalpy of Formation of Hydrocarbons and Hydrocarbon Radicals, *The Journal of Physical Chemistry A* 109 (2005) 7466-7480.
- [59] J. Jian, H. Hashemi, H. Wu, A.W. Jasper, P. Glarborg, A reaction mechanism for ozone dissociation and reaction with hydrogen at elevated temperature, *Fuel* 322 (2022) 124138.
- [60] H. Wang, M. Frenklach, Transport properties of polycyclic aromatic hydrocarbons for flame modeling, *Combustion and Flame* 96 (1994) 163-170.
- [61] G. Vanhove, Y. Yu, M.A. Boumehdi, O. Frottier, O. Herbinet, P.-A. Glaude, F. Battin-Leclerc, Experimental Study of Tetrahydrofuran Oxidation and Ignition in Low-Temperature Conditions, *Energy & Fuels* 29 (2015) 6118-6125.
- [62] H. Song, R. Dauphin, G. Vanhove, A kinetic investigation on the synergistic low-temperature reactivity, antagonistic RON blending of high-octane fuels: Diisobutylene and cyclopentane, *Combustion and Flame* 220 (2020) 23-33.